Doctor's Thesis

Chaos Analysis of Heart Rate Variability and Experimental Verification of Hypotheses Based on the Neurovisceral Integration Model

Guidance
Ken Umeno

Tomoyuki Mao

Department of Applied Mathematics and Physics
Graduate School of Informatics
Kyoto University

February 2023

Contents

Chapter 1

Introduction

1.1 Estimation of physiological state

Stress can be a factor in various illnesses, including mental illnesses such as depression. Fatigue and drowsiness can also lead to serious traffic accidents, especially for professional drivers. Examples of serious accidents caused by overworked or drowsy drivers include the 2007 Suita ski bus accident (1 fatality), the 2012 Kanetsu Expressway highway bus accident (7 fatalities), and the 2016 Karuizawa ski bus accident (15 fatalities). Therefore, it is necessary to estimate physiological states such as stress, fatigue, and drowsiness in order to protect people ' s health and safety.

The difficulty in physiological state estimation lies in the difficulty of measuring and quantifying human internal states. Considering clinical and general applications, a method that is easy to perform, non-invasive, quick, and low-cost is required. Estimation of physiological status by non-invasive and quantitative methods is an important issue. Heart rate variability analysis has attracted attention as one of the methods that may lead to physiological state estimation.

1.2 Heart rate variability and autonomic nervous system

The autonomic nervous system is involved in the regulation of the heart. The sympathetic nerves accelerate the heartbeat and the parasympathetic nerves decelerate the heartbeat. These sympathetic and parasympathetic nervous activities cause fluctuations in the interval of heart beats (R-R Interval : RRI) [1, 2]. This phenomenon is called heart rate variability (HRV). Fig. 1.1 shows a schematic diagram of the electrocardiogram (ECG) waveform and R-R Interval (RRI). Fig.

1.2 illustrates an example of the fluctuation of a typical RRI time series.

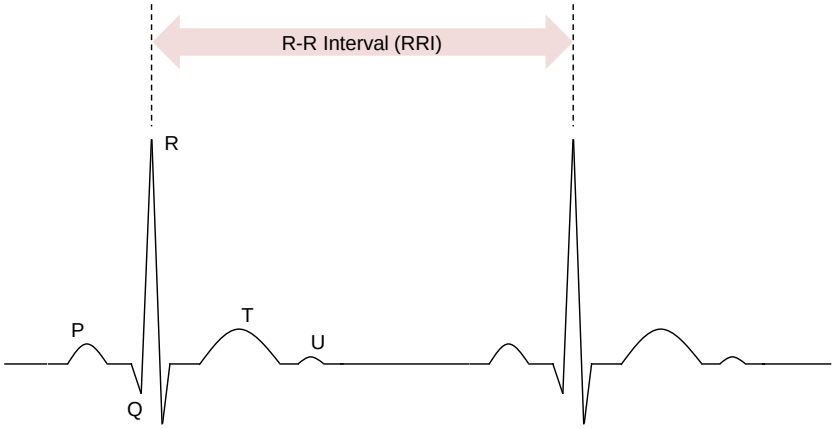

Figure 1.1: Schematic picture of a basic electrocardiogram (ECG) waveform; the time interval from the peak labeled R to the R of the next beat is called the R-R Interval (RRI).

RRI data can be measured by the change in the potential difference on the skin surface associated with the beating of the heart. Recently, wearable heart rate sensors have been developed to easily and continuously measure RRI data.

There are methods to quantitatively evaluate autonomic nervous system function by analyzing R-R interval data. Heart rate variability analysis is a powerful method for noninvasively examining the internal state of human body.

1.3 Chaotic nature of heart rate variability and nonlinear analysis

The method for evaluating autonomic nervous system function by heart rate variability analysis was standardized in 1996 [3] and consists of two types of analysis: time-domain analysis (analysis by statistics) and frequency-domain analysis (analysis by power of specific frequency components).

However, the two conventional analytic methods do not evaluate fluctuations in heartbeat intervals from the perspective of dynamics. It has been pointed out that these linear analyses can only capture some aspects of heart rate variability and have limitations in analyzing biological phenomena that are nonlinear systems [4]. Aspects of heart rate variability not captured by conventional linear analysis have not yet been fully understood, and are therefore variously referred to as chaos, nonlinear components, fractal components, and so on in the literature. In this study, we consider them as chaos.

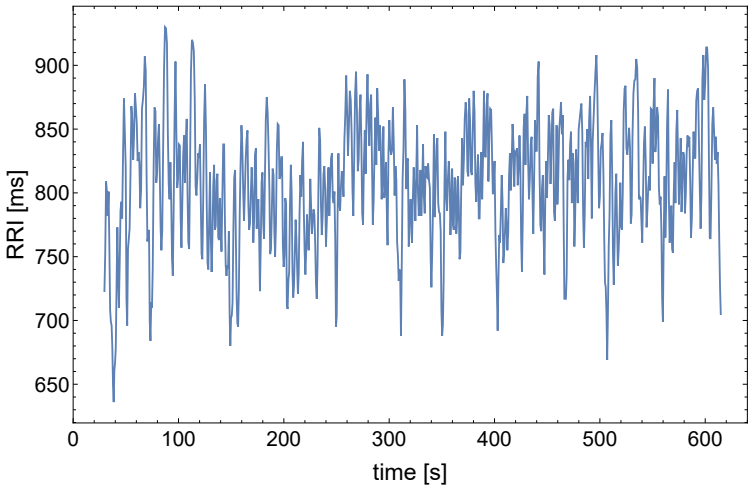

Figure 1.2: Example of a typical RRI time series. In a healthy heart, the RRI is not constant but fluctuates.

Deterministic chaos is a phenomenon in which a system is deterministic but exhibits irregular behavior that appears as if it were stochastic. One of the characteristic and interesting properties of chaos is its sensitivity to initial conditions, in which small differences in initial values expand over time to make large differences in future outcomes, and its unpredictability in the long term, even though a system follows deterministic laws. Although the discovery of chaos was made through studies of electric circuits and meteorology, chaos is considered to be a kind of universal property that is also related to a wide variety of other phenomena, including life sciences and financial markets. Therefore, there is a great potential to highlight the characteristics of the mechanism of heart rate control hidden in the seemingly random RRI variation as shown in Fig. 1.2 from the perspective of chaos.

Recently, experiments using complexity indices such as entropy have reported a relationship between the complexity of heart rate variability and cognitive function and mood (anxiety) [5, 6, 7, 8]. Thus, nonlinear analysis of heart rate variability is revealing aspects that were invisible to conventional linear analysis. For example, finding signs of heart disease or sudden death remains a major challenge [9], and nonlinear analysis may be one approach to such problems. Furthermore, it has been reported that nonlinear analysis can detect the increased sympathetic modulation in breast cancer patients after initial treatment that cannot be detected by linear analysis of HRV [10]. It is expected that nonlinear analysis of HRV will be applied to clinical practice.

1.4 Methods for Quantifying Chaos

The Lyapunov exponent is commonly used to quantify chaos. It is a measure of sensitive dependence on initial conditions, which is a typical property of chaos (the property that slight differences in initial values increase exponentially over time, resulting in large changes in trajectory). If the Lyapunov exponent is positive in a system, the system is judged to be chaotic; conversely, if it is negative, the system is stable and not chaotic.

Representative methods for estimating Lyapunov exponents from time series data based on the reconstruction of attractors by delay coordinates embedding [11] include the methods by Wolf *et al.*[12], Rosenstein *et al.*[13], and Kantz[14]. However, methods for estimating Lyapunov exponents from observed data series, including the methods listed above, face some challenges, such as the need for the equations of the dynamical system generating the data, the need for large amounts of data and computation, and the need to properly select computational parameters such as delay time and embedding dimension. This means that it is difficult to use Lyapunov exponent in applications where heart rate variability is analyzed in real time. This is because there are no explicit equations that describe the system that produces heart rate variability, and because the RRI data is only available at the timing of beats, thus if we assume that the measurement time is 5 minutes, there are only a few hundred data points in the data set.

The chaos degree [15] has been proposed as a measure of chaos from only a sequence of observed data and from a relatively small amount of data. It measures the amount of information that chaos generates from an information-theoretic perspective. In this study, we position the chaos degree as a quantification index of chaos similar to the Lyapunov exponent and attempt to apply it as an effective means of measuring chaos in heart rate variability analysis.

1.5 Issues addressed in this study

There are two major problems in translating the nonlinear analysis of HRV into useful applications.

First, there are still no indices that can be considered standard in nonlinear analysis of HRV. The conclusions of previous studies listed above differ slightly due to the slightly different objectives and conditions of the experiments and the fact that not all experiments used the same analytical methods. Improved chaos degree proposed in this study is considered appropriate as an index to quantify the chaos of heart rate variability. Improved chaos degree can be calculated from data, requires little computation, and has a clear mathematical correspondence with Lyapunov exponent.

Second, there is still no clear explanation of what is essentially meant by chaos/complexity in heart rate variability. As an approach to the question, we hypothesize that the chaos in heart rate variability reflects the effects of brain network activity and attempt to verify part of this hypothesis through experimentation.

1.6 Outline of the thesis

In this thesis, in the first half (Chapters 2 and 3), we propose a quantification index of chaos that can be computed from data and has a clear mathematical background. In the second half (Chapters 4 and 5), we derive the hypothesis that the chaos of heart rate variability is affected by higher-order brain activity, and conduct experiments to verify the hypotheses, and apply the chaos index proposed in the first half to the analysis of experimental data.

In Chapter 2, we examine the properties of chaos degree using asymmetric tent maps, focusing on the difference between chaos degree and Lyapunov exponent, and give an information-theoretic interpretation of the difference between them. Furthermore, we derive analytically the limit of the infinite number of divisions of chaos degree.

In Chapter 3, we define improved chaos degree as chaos degree from which the amount of information that is the difference between chaos degree and Lyapunov exponent is removed and prove that improved chaos degree is consistent with discretized Lyapunov exponent.

In Chapter 4, we summarize previous studies on the neuroviceral integration model that explain the relationship between higher brain functions and heart rate control, and previous studies on large-scale brain networks, and add our own considerations from the perspective of chaos to formulate hypotheses linking chaos in heart rate variability and higher brain activity.

In Chapter 5, we conduct experiments to analyze heart rate variability data during brain activities (mental arithmetic and Sudoku) to verify our hypotheses.

Chapter 2

Investigation of properties of chaos degree

This chapter is according to the [16] and [17].

2.1 Introduction

Lyapunov exponent is commonly used as a quantitative measure of chaos. However, it is difficult to calculate Lyapunov exponents if equations of dynamical systems are not given. On the other hand, Entropic Chaos Degree (chaos degree) [15] is proposed as another measure of chaos which can be directly calculated from data. The properties of chaos degree and its relationship with other chaos indicators have been investigated and discussed in previous studies [18, 19, 20, 21].

The advantage of chaos degree is that it can be computed from only data series and with a small amount of computation. In this thesis, chaos degree is positioned as a suitable index for quantifying the chaotic nature of heart rate variability, but it has an extremely wide range of applications because it can be applied to general data, not limited to HRV data.

In order to apply chaos degree to the analysis of real data, it is necessary to clarify its basic properties, such as its relationship with Lyapunov exponent. In this chapter, we investigate the properties of chaos degree using asymmetric tent map as a simple model of chaotic dynamical systems. The value of chaos degree is affected by the partition used in its computation. In the first half of the chapter, we investigate the difference between chaos degree and Lyapunov exponent caused by the effect of the partition, and in the second half of the chapter, we obtain analytically chaos degree in the limit of infinite number of partitions.

2.2 Analysis of the difference between chaos degree and Lyapunov exponent in asymmetric tent maps, and information-theoretic interpretation of the difference

2.2.1 Introduction

Relations among chaos degree, Lyapunov exponent and KS entropy are discussed in [21]. Previous research [22] analytically shows that chaos degree in the limit that partition number approaches to infinity is *greater* than Lyapunov exponent, and suggests that the difference between chaos degree and Lyapunov exponent depends on the choice of partition. In many cases, chaos degree is greater than Lyapunov exponent and we should be careful to determine chaos by using chaos degree. For example, preceding studies[19, 20] show that chaos degree is positive for quasi-periodic orbits and it is hard to distinguish chaotic orbits from quasi-periodic orbits.

This section reports on an analytical investigation of the difference between chaos degree and Lyapunov exponent for asymmetric tent maps.

2.2.2 Definition of Chaos Degree

The definition of chaos degree in difference equations is as below.

We assume that the difference equation is determined by a map $f : I \to I$ ($\equiv [a, b]^d \subset \mathbf{R}^d$, $a, b \in \mathbf{R}, d \in \mathbf{N}$), i.e., $x_{n+1} = f(x_n)$ $(n = 0, 1, \ldots)$. Let x_0 be an initial value, and $A = \{A_i\}$ be a finit partition of I such that

$$I = \bigcup_{k=1}^{N} A_k, \ A_i \cap A_j = \emptyset \ \ (i \neq j). \tag{2.2.1}$$

The probability distribution $p_{i,A}^{(m)}(M)$ at the time m is given as

$$p_{i,A}^{(m)}(M) = \frac{1}{M} \sum_{k=m}^{m+M-1} 1_{A_i}(x_k), \tag{2.2.2}$$

and the joint probability distribution $p_{i,j,A}^{(m,m+1)}(M)$ between the time m and $m+1$ is given as

$$p_{i,j,A}^{(m,m+1)}(M) = \frac{1}{M} \sum_{k=m}^{m+M-1} 1_{A_i}(x_k) 1_{A_j}(x_{k+1}). \tag{2.2.3}$$

Then chaos degree $D^{(M,m)}(A, f)$ for the orbit $\{x_k\}$ is defined by

$$D^{(M,m)}(A, f) = \sum_{i=1}^{N}\sum_{j=1}^{N} p_{i,j,A}^{(m,m+1)}(M) \log \frac{p_{i,A}^{(m)}(M)}{p_{i,j,A}^{(m,m+1)}(M)}. \tag{2.2.4}$$

In this paper, we simplify $p_{i,A}^{(m)}(M) = p(i)$ and $p_{i,j,A}^{(m,m+1)}(M) = p(i, j)$, then chaos degree H_{CD} is calculated as:

$$H_{CD} = \sum_{i=1}^{N}\sum_{j=1}^{N} p(i, j) \log \frac{p(i)}{p(i, j)} \tag{2.2.5}$$

$$= -\sum_{i=1}^{N} p(i) \sum_{j=1}^{N} p(j|i) \log p(j|i), \tag{2.2.6}$$

where the conditional probability $p(j|i) = \dfrac{p(i, j)}{p(i)}$.

2.2.3 Asymmetric tent map

Let $T_k(x)$ be a tent map with the peak at $x = 1/k$ ($k \in \mathbf{N}$, $k \geq 2$) such that

$$T_k(x) = \begin{cases} kx & (0 \leq x \leq \frac{1}{k}) \\ \frac{k}{k-1}(1 - x) & (\frac{1}{k} \leq x \leq 1) \end{cases}. \tag{2.2.7}$$

If $k = 2$ then $T_k(x)$ is a *symmetric* tent map, else $T_k(x)$ is an *asymmetric* tent map.

We try to find out how partitions affect the difference between chaos degree and Lyapunov exponent, focusing on asymmetric tent map $T_k(x)$ because its shape is simple so that it is easy to calculate both theoritical values of chaos degree and Lyapunov exponents.

2.2.4 Investigation prosedure

First, we calculate chaos degree of an asymmetric tent map $T_k(x)$. Next, we claculate a difference between chaos degree and Lyapunov Exponent ($H_{CD} - \lambda$) and try to interpret what the difference means.

2.2.5 Calculation of Chaos Degree

Let $\{A_i\}$ be an equipartition with partition number N such that $N = nk$ ($n \in \mathbf{N}$). For example, the case $k = 4$ and $n = 2$ is shown in Fig. 2.1.

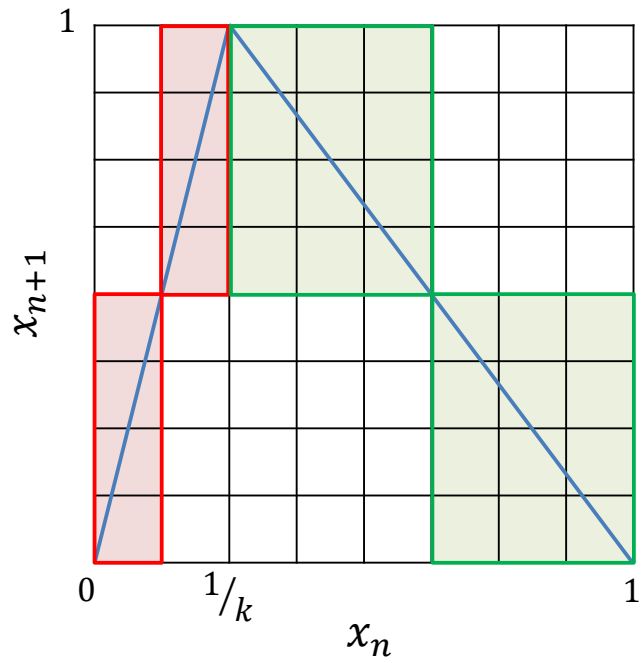

Figure 2.1: Example of an asymmetric tent map $T_k(x)$ and an nk equipartition for $k = 4$ and $n = 2$.

There are two kinds of repeating patterns in $0 \leq x \leq \frac{1}{k}$ and $\frac{1}{k} \leq x \leq 1$. In Fig. 2.1, each pattern is colored red or green. Each of these patterns appears n times.

If (A_i, A_j) such that $x_m \in A_i$ and $x_{m+1} \in A_j$ does not belong to any patterns, then $p(j|i) = 0$ and chaos degree is not affected. Therefore, we consider the two patterns in calculation of chaos degree below.

In case $0 \leq x \leq \frac{1}{k}$, $T_k(A_{i_1})$ intersects with just k components, therefore conditional probability is

$$p(j|i_1) = \begin{cases} \frac{1}{k} & (j = j_1, j_2, \ldots j_k) \\ 0 & (otherwise) \end{cases} . \tag{2.2.8}$$

In case $\frac{1}{k} \leq x \leq 1$, each of $T_k(A_{i_u})$ $(u = 1, 2, \ldots k-1)$ intersects with just two components. Suppose the index numbers of the two components are v_1 and v_2, then

$$p(j|i_u) = \begin{cases} \frac{u}{k} & (j = j_{v_1}) \\ \frac{k-u}{k} & (j = j_{v_2}) \\ 0 & (otherwise) \end{cases} . \tag{2.2.9}$$

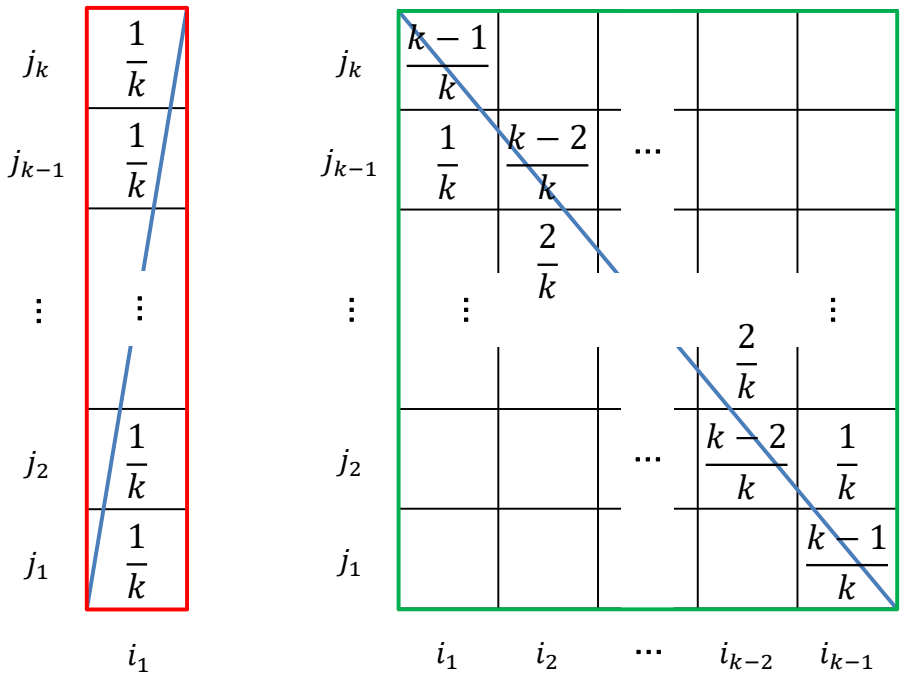

(a) $0 \le x \le \frac{1}{k}$ (b) $\frac{1}{k} \le x \le 1$

Figure 2.2: Schematic picture of two kinds of repeating patterns and conditional probability $p(j|i)$. In pattern (b), $p(j|i) = 0$ is omitted.

Futher, $T_k(x)$ has the uniform invariant probability density, therefore

$$p(i) = \frac{1}{N} = \frac{1}{nk}. \tag{2.2.10}$$

From equations (3.2.6), (2.2.8), (2.2.9) and (2.2.10), we obtain

$$\begin{aligned} & H_{CD} \\ & = \frac{1}{nk} nk \left(-\frac{1}{k} \log \frac{1}{k} \right) \\ & \quad + \frac{1}{nk} n \sum_{u=1}^{k-1} \left(-\frac{u}{k} \log \frac{u}{k} - \frac{k-u}{k} \log \frac{k-u}{k} \right) \\ & = -\frac{1}{k} \log \frac{1}{k} \\ & \quad + \frac{1}{k} \sum_{u=1}^{k-1} \left(-\frac{u}{k} \log \frac{u}{k} - \frac{k-u}{k} \log \frac{k-u}{k} \right). \end{aligned} \tag{2.2.11}$$

Note that H_{CD} does not depend on n.

2.2.6 Calculation of the difference between Chaos Degree and Lyapunov Exponent

Lyapunov exponent λ is given as

$$\lambda = -\frac{1}{k} \log \frac{1}{k} - \frac{k-1}{k} \log \frac{k-1}{k}. \tag{2.2.12}$$

Chaos degree H_{CD} for $k \geq 2$ and Lyapunov exponent λ is shown in Fig. 2.3. The horizontal axis a is the peak of $T_k(x)$ i.e. $a = \frac{1}{k}$. As can be seen from the figure, when $k = 2$ ($a = \frac{1}{2}$; $T_k(x)$ is a symmetric tent map), chaos degree equals Lyapunov exponent, and in other cases, chaos degree is *greater* than Lyapunov exponent.

Theorem 1. *Let $T_k(x)$ be an asymmetric tent map which is given by equation (2.3.7) and $\{A_i\}$ be an nk equipartition of $I = [0, 1]$, then we have*

$$H_{CD} \geq \lambda, \tag{2.2.13}$$

where H_{CD} is chaos degree and λ is Lyapunov exponent.

Proof. From equations (2.2.11) and (2.2.12), the difference between chaos degree and Lyapunov exponent can be calculated as follows:

$$\begin{aligned}
&H_{CD} - \lambda \\
&= \frac{1}{k}\sum_{u=1}^{k-1}\left(-\frac{u}{k}\log\frac{u}{k} - \frac{k-u}{k}\log\frac{k-u}{k}\right) \\
&\quad -\left(-\frac{k-1}{k}\log\frac{k-1}{k}\right) \\
&= \frac{1}{k}\sum_{u=1}^{k-1}\left(-\frac{u}{k}\log\frac{u}{k} - \frac{k-u}{k}\log\frac{k-u}{k}\right) \\
&\quad +\frac{1}{k}\sum_{u=1}^{k-1}\log\frac{k-1}{k} \\
&= \frac{1}{k}\sum_{u=1}^{k-1}\left(-\frac{u}{k}\log\frac{u}{k-1} - \frac{k-u}{k}\log\frac{k-u}{k-1}\right).
\end{aligned} \tag{2.2.14}$$

Thus, we have $H_{CD} - \lambda \geq 0$, i.e. $H_{CD} \geq \lambda$. The equality holds for $k = 2$ (symmetric tent map case). □

The difference between chaos degree and Lyapunov Exponent is shown in Fig. 2.4. The horizontal axis a is the peak of $T_k(x)$ i.e. $a = \frac{1}{k}$. When $a = 0$, although Lyapunov exponent $\lambda = 0$, the difference $H_{CD} - \lambda$ is maximum. This shows that it is difficult to determine chaos for weak chaos by using chaos degree H_{CD}.

Fig. 2.4 also shows that values of the difference $H_{CD} - \lambda$ are close to the line $-a + \frac{1}{2}$. We can understand this behavior as below. From equation (2.2.14),

$$\begin{aligned}
&H_{CD} - \lambda \\
&= \frac{1}{k}\sum_{u=1}^{k-1}\left(-\frac{u}{k}\log\frac{u}{k-1} - \frac{k-u}{k}\log\frac{k-u}{k-1}\right) \\
&= 2\left(1-\frac{1}{k}\right)^2\sum_{u=1}^{k-1}\left(-\frac{u}{k-1}\log\frac{u}{k-1}\right)\frac{1}{k-1}.
\end{aligned} \tag{2.2.15}$$

For sufficiently large k,

$$\begin{aligned}
H_{CD} - \lambda &\sim 2\left(1-\frac{2}{k}\right)\int_0^1 (-x\log x)dx \\
&= -a + \frac{1}{2}.
\end{aligned} \tag{2.2.16}$$

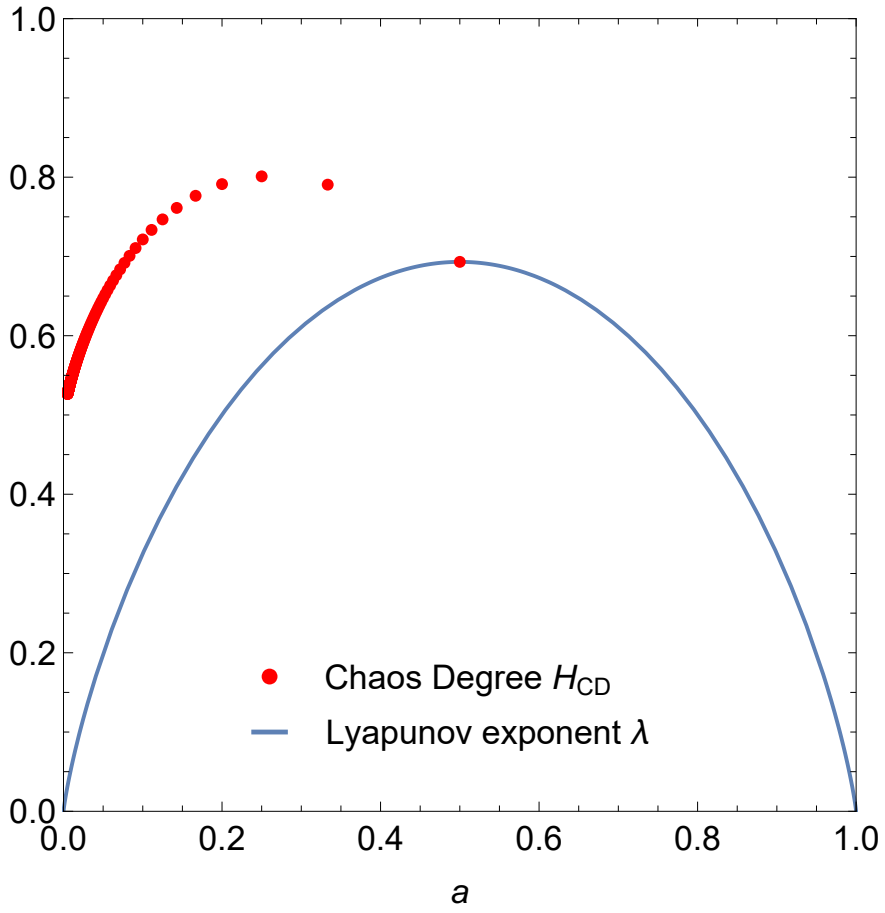

Figure 2.3: Chaos degree and Lyapunov exponent of asymmetric tent map $T_k(x)$.

2.2.7 Interpretation of the difference

Theorem 2. *Suppose that $T_k(x)$ is an asymmetric tent map and $\{A_i\}$ is an nk equipartition of $I = [0, 1]$. The difference between chaos degree and Lyapunov exponent $H_{CD} - \lambda$ can be calculated as an average of some kind of information $-\log q(i, j)$, where $q(i, j)$ is defined as*

$$q(i, j) \overset{\text{def}}{=} \frac{\|T_k(A_i) \cap A_j\|}{\|A_j\|}. \tag{2.2.17}$$

Proof. Since $\{A_i\}$ is an nk equipartition,

$$\|A_i\| = \Delta = \frac{1}{nk} \ (i = 1, 2, \ldots, N). \tag{2.2.18}$$

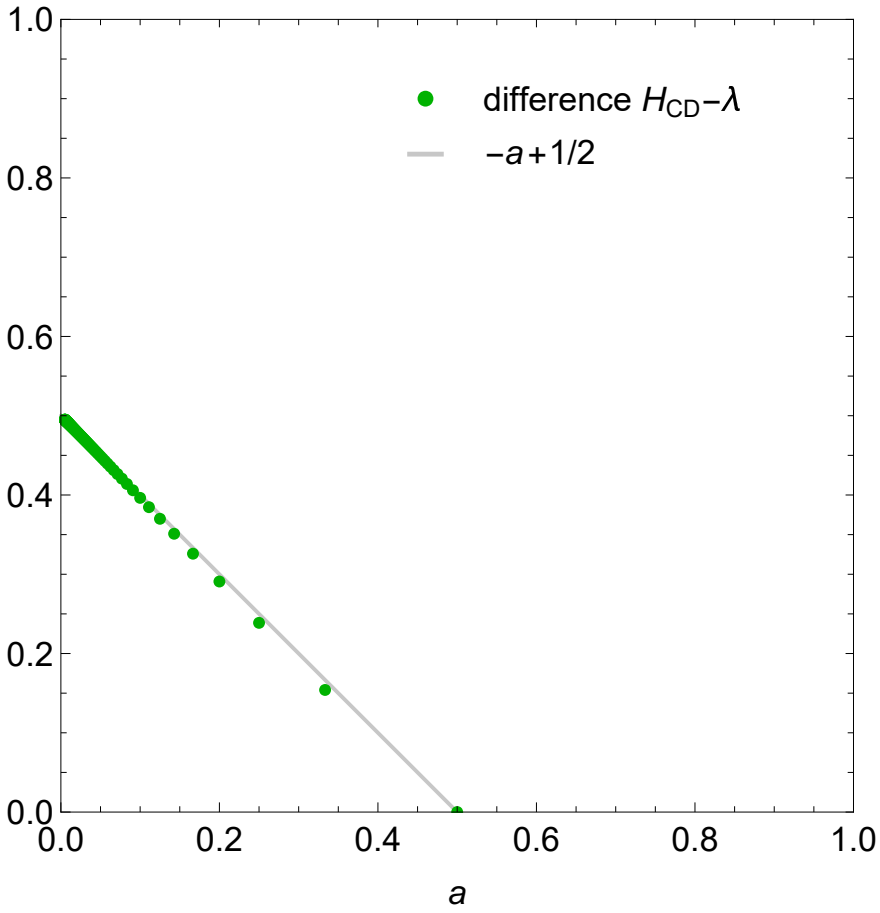

Figure 2.4: The difference between chaos degree and Lyapunov exponent ($H_{CD}-\lambda$) with the line $-a+\frac{1}{2}$.

In case $0 \leq x \leq \frac{1}{k}$,

$$q(i_1, j) = \frac{\|A_j\|}{\|A_j\|} = 1 \quad (j = j_1, j_2, \ldots j_k). \tag{2.2.19}$$

In case $\frac{1}{k} \leq x \leq 1$, as shown in Fig. 2.5 ,

$$q(i_u, j) = \begin{cases} \frac{u}{k-1} & (j = j_{v_1}) \\ \frac{k-u}{k-1} & (j = j_{v_2}) \\ 0 & (otherwise) \end{cases}. \tag{2.2.20}$$

Therefore, the difference $H_{CD} - \lambda$ is calculated as:

$$\begin{aligned} & H_{CD} - \lambda \\ &= \frac{1}{k} \sum_{u=1}^{k-1} \left(-\frac{u}{k} \log \frac{u}{k-1} - \frac{k-u}{k} \log \frac{k-u}{k-1} \right) \\ &= \frac{1}{nk} n \sum_{u=1}^{k-1} \left(-p(j_{v_1}|i_u) \log q(i_u, j_{v_1}) \right. \\ &\qquad \left. -p(j_{v_2}|i_u) \log q(i_u, j_{v_2}) \right) \\ &= \frac{1}{nk} n \sum_{u=1}^{k-1} \left(\sum_{v=1}^{k} p(j_v|i_u) \{ -\log q(i_u, j_v) \} \right) \\ &= \frac{1}{nk} \sum_{i=1}^{N} \left(\sum_{j=1}^{N} p(j|i) \{ -\log q(i, j) \} \right) \\ &= \sum_{i=1}^{N} p(i) \sum_{j=1}^{N} p(j|i) \{ -\log q(i, j) \}. \end{aligned} \tag{2.2.21}$$

□

If we regard $-\log q(i, j)$ as an amount of information, equation (2.2.21) is intuitively interpreted as below. When we assume that T_k maps A_i, chaos degree is calculated by entropy of conditional probability $p(j|i)$, then chaos degree is the same value in the case that the output is *uniformly* distributed in the whole of A_j and is greater than Lyapunov exponent. This difference is owing to lack of consideration about how output is distributed in each A_j. An actual distribution of output is limited in $T_k(A_i) \cap A_j$ and entropy should be *less* than the value in the case that output is distributed in whole of A_j. We can assume that this is because the entropy is added with $-\log q(i, j)$, which is an amount of information necessary to know that output is in $T_k(A_i) \cap A_j$.

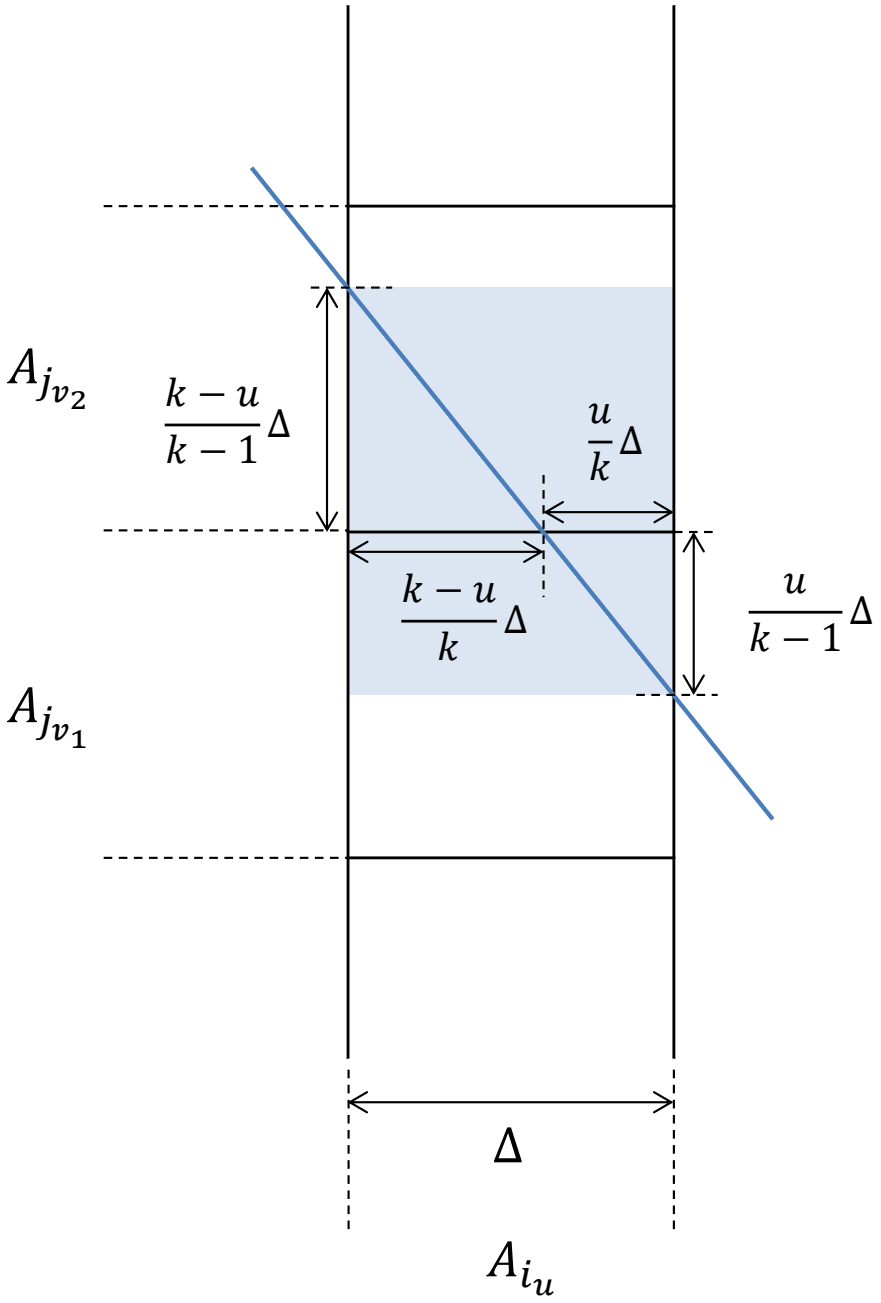

Figure 2.5: Figure of intersection between $T_k(A_{i_u})$ and two components $A_{j_{v_1}}, A_{j_{v_2}}$.

2.2.8 Conclusion

We try to interpret the difference between chaos degree and Lyapunov exponent for asymmetric tent maps and find out that the difference $H_{CD} - \lambda$ can be calculated as an average of some kind of information $-\log q(i, j)$ and thus be non-negative. It is assumed that information $-\log q(i, j)$ is related to intersection of mapping $T_k(x)$ and components of partition $\{A_i\}$.

2.3 Analysis of the limit values of chaos degree for infinite number of partitions in asymmetric tent maps

2.3.1 Introduction

It is known that the values of chaos degree are affected by the partitioning in the process of their computation. We investigated the effect of partitioning on chaos degree of asymmetric tent maps in the simple case with certain restricted parameters and the number of partitions in the previous study [16]. Furthermore, we interpreted the difference between chaos degree and Lyapunov exponent caused by the effect of partitioning in information-theoretic terms, and defined improved chaos degree [23] as chaos degree subtracted by the difference.

The theoretical upper bound of chaos degree including the effect of partitions is given by $\log N$ (where N is the number of partitions), but it is not obvious whether the limit of chaos degree with N at infinity diverges, converges, or not. In this section, we generalize the parameters of asymmetric tent maps to real numbers $a(> 1)$ and obtain analytically chaos degree in the limit of infinite number of partitions.

2.3.2 Definition of chaos degree

The definition of chaos degree in difference equations is as below.

We assume that the difference equation is determined by a map $f : I \to I$ ($\equiv [a, b]^d \subset \mathbf{R}^d$, $a, b \in \mathbf{R}, d \in \mathbf{N}$), i.e., $x_{n+1} = f(x_n)$ $(n = 0, 1, \ldots)$. Let x_0 be an initial value, and $A = \{A_i\}$ be a finit partition of I such that

$$I = \bigcup_{k=1}^{N} A_k, \ A_i \cap A_j = \emptyset \ \ (i \neq j). \tag{2.3.1}$$

The probability distribution $p_{i,A}^{(m)}(M)$ at the time m is given as

$$p_{i,A}^{(m)}(M) = \frac{1}{M} \sum_{k=m}^{m+M-1} 1_{A_i}(x_k), \tag{2.3.2}$$

and the joint probability distribution $p_{i,j,A}^{(m,m+1)}(M)$ between the time m and $m+1$ is given as

$$p_{i,j,A}^{(m,m+1)}(M) = \frac{1}{M} \sum_{k=m}^{m+M-1} 1_{A_i}(x_k) 1_{A_j}(x_{k+1}). \tag{2.3.3}$$

Then chaos degree $D^{(M,m)}(A, f)$ for the orbit $\{x_k\}$ is defined by

$$\begin{aligned} &D^{(M,m)}(A, f) \\ &= \sum_{i=1}^{N} \sum_{j=1}^{N} p_{i,j,A}^{(m,m+1)}(M) \log \frac{p_{i,A}^{(m)}(M)}{p_{i,j,A}^{(m,m+1)}(M)}. \end{aligned} \tag{2.3.4}$$

In this paper, we simplify as $p_{i,A}^{(m)}(M) = p(i)$ and $p_{i,j,A}^{(m,m+1)}(M) = p(i,j)$, then chaos degree H_{CD} is calculated as:

$$H_{CD} = \sum_{i=1}^{N} \sum_{j=1}^{N} p(i,j) \log \frac{p(i)}{p(i,j)} \tag{2.3.5}$$

$$= -\sum_{i=1}^{N} p(i) \sum_{j=1}^{N} p(j|i) \log p(j|i), \tag{2.3.6}$$

where the conditional probability is given by $p(j|i) = \dfrac{p(i,j)}{p(i)}$.

2.3.3 Asymmetric tent map

Let $T_a(x)$ be a tent map with the peak at $x = 1/a$ ($a \in \mathbf{R}$, $a > 1$) such that

$$T_a(x) = \begin{cases} f_{L,a}(x) = ax & \left(0 \le x \le \dfrac{1}{a}\right) \\ f_{R,a}(x) = \dfrac{a}{a-1}(1-x) & \left(\dfrac{1}{a} \le x \le 1\right) \end{cases}. \tag{2.3.7}$$

If $a = 2$ then $T_a(x)$ is a *symmetric* tent map, else $T_a(x)$ is an *asymmetric* tent map.

Let us call the part of $T_a(x)$ to the left of the peak the left-hand side function $f_{L,a}(x)$ and the part to the right of the peak the right-hand side function $f_{R,a}(x)$.

The asymmetric tent map $T_a(x)$ is ergodic and, as an invariant measure $\rho(x)$, has a uniform distribution regardless of a, i.e. $\rho(x) = 1$.

2.3.4 Calculation of the limit values of chaos degree

Let the finite partition $\{A_i\}$ be N-equipartition. That is,

$$A_i = [(i-1)\Delta x, i\Delta x], \tag{2.3.8}$$

$$\Delta x = 1/N. \tag{2.3.9}$$

In computing the limit of chaos degree for the number of partitions $N \to \infty$, we distinguish between the right side and the left side of the vertex. Only when summing over i in the right-hand region, we use a new number i' assigned from the right instead of the interval number i to apply the same argument as on the left-hand region (Fig. 2.6). The numbering of j starts from the origin and goes $1, 2, 3.....$ Note that there is at most one interval containing the vertex among the N partitions, but because it will not contribute to the limit of $N \to \infty$, it will be ignored in the following discussion.

Let the entropy of the conditional probability per component of the partition be the partition entropy, that is,

$$h(i) = -\sum_{j=1}^{N} p(j|i) \log p(j|i). \tag{2.3.10}$$

On the right side of the vertex, i' is used instead of the number i, but it is denoted as i here because the discussion below is the same for both the left and right sides. Let α be the slope of an asymmetric tent map $T_a(x)$ on some interval A_i. The intersection of the segment A_j and a line starting at the origin with slope α is shown in Fig. 2.7. The conditional probability $p(j|i)$ for computing the partition entropy $h(i)$ can be obtained for each of the following three cases A, B and C. First, the case A is the case where j is the largest among the intervals A_j that intersect the mapping (the topmost interval in Fig. 2.7). In this case, if $j = j_A$, the width of $A_{j_A} \cap T_a(A_i)$ is $(i\alpha - \lfloor i\alpha \rfloor)\Delta x$, and the conditional probability

$$p(j_A|i) = \frac{(i\alpha - \lfloor i\alpha \rfloor)\Delta x}{\alpha \Delta x} = \frac{(i\alpha - \lfloor i\alpha \rfloor)}{\alpha}. \tag{2.3.11}$$

Next, consider the case C in which j is the smallest among the intervals A_j that intersect the mapping. In this case, if $j = j_C$, the width of $A_{j_C} \cap T_a(A_i)$ is $\{1 - \{(i-1)\alpha - \lfloor (i-1)\alpha \rfloor\}\}\Delta x$, and the conditional probability

$$\begin{aligned} p(j_C|i) &= \frac{\{1 - \{(i-1)\alpha - \lfloor (i-1)\alpha \rfloor\}\}\Delta x}{\alpha \Delta x} \\ &= \frac{\{1 - \{(i-1)\alpha - \lfloor (i-1)\alpha \rfloor\}\}}{\alpha}. \end{aligned} \tag{2.3.12}$$

Finally, considering each interval between cases A and C such that $j = j_B (j_C < j_B < j_A)$ as case B, the conditional probability

$$p(j_B|i) = \frac{\Delta x}{\alpha \Delta x} = \frac{1}{\alpha} \tag{2.3.13}$$

because $A_{j_B} \cap T_a(A_i) = A_{j_B}$. There are $\lfloor i\alpha \rfloor - \lfloor (i-1)\alpha \rfloor - 1$ intervals that correspond to case B. Therefore, the partition entropy

$$\begin{aligned} h(i) =& - p(j_A|i) \log p(j_A|i) - p(j_C|i) \log p(j_C|i) \\ & + (\lfloor i\alpha \rfloor - \lfloor (i-1)\alpha \rfloor - 1)(-p(j_B|i) \log p(j_B|i)) \\ =& - \log \frac{1}{\alpha} - \frac{1}{\alpha} \langle i\alpha \rangle \log \langle i\alpha \rangle \\ & - \frac{1}{\alpha} \{1 - \langle (i-1)\alpha \rangle\} \log \{1 - \langle (i-1)\alpha \rangle\}. \end{aligned} \tag{2.3.14}$$

Note that the symbol $\langle \alpha \rangle$ is used to denote the fractional part of α. That is, $\langle \alpha \rangle = \alpha - \lfloor \alpha \rfloor$.

In order to obtain the limit value of chaos degree

$$H_{CD} = \sum_{i=1}^{N} p(i) h(i) \tag{2.3.15}$$

with infinite number of partitions, we focus on the distribution of the fractional part $\langle i\alpha \rangle$ of $i\alpha$.

The following theorem holds for the distribution of $\langle i\alpha \rangle$.

Theorem 3. *The series S formed by $\langle i\alpha \rangle = i\alpha - \lfloor i\alpha \rfloor$, the fractional part of $i\alpha$ for $i \in \mathbf{N}$, has a continuous uniform distribution over $[0, 1)$ when α is an irrational number, and a discrete uniform distribution over $X = \{\frac{0}{m}, \frac{1}{m}, \frac{2}{m}, ..., \frac{m-1}{m}\}$ when α is a rational number $\frac{n}{m}$ (n and m are prime to each other).*

Proof. When α is an irrational number, from Kronecker's approximation theorem and Weyl's equidistribution theorem [24], S has a continuous uniform distribution over $[0, 1)$.

When α is a rational number, the possible values of the series S are limited to $X = \{\frac{0}{m}, \frac{1}{m}, \frac{2}{m}, ..., \frac{m-1}{m}\}$ because

$$\left\langle i \frac{n}{m} \right\rangle = \frac{in \bmod m}{m}. \tag{2.3.16}$$

S has period m, because

$$\left\langle (i+m) \frac{n}{m} \right\rangle = \left\langle i \frac{n}{m} \right\rangle. \tag{2.3.17}$$

Furthermore, in one period ($i = 1, 2, ..., m$), S contains m elements in X without duplication, because $i \not\equiv j \mod m \Rightarrow in \not\equiv jn \mod m$ ($\because n$ and m are prime to each other). Therefore, the series S has a discrete uniform distribution over X. □

Based on Theorem 3, the following theorem holds for the limit of chaos degree with infinite number of partitions.

Theorem 4. *When the parameter a (> 1) is an irrational number, the limit value of chaos degree of the asymmetric tent map $T_a(x)$ for the partition number $N \to \infty$ using N-equipartition is as*

$$\lim_{N\to\infty} H_{CD} = -\frac{1}{a}\log\frac{1}{a} - \frac{a-1}{a}\log\frac{a-1}{a} + \frac{1+(a-1)^2}{2a^2}.$$

On the other hand, when a is a rational number $a = \frac{n}{m}$ (n and m are prime to each other), the limit value is as

$$\begin{aligned}\lim_{N\to\infty} H_{CD} = &-\frac{m}{n}\log\frac{m}{n} - \frac{n-m}{n}\log\frac{n-m}{n} \\ &+ \frac{2m}{n^2}\sum_{i=0}^{m-1}\left(-\frac{i}{m}\log\frac{i}{m}\right) \\ &+ \frac{2(n-m)}{n^2}\sum_{i=0}^{n-m-1}\left(-\frac{i}{n-m}\log\frac{i}{n-m}\right)\end{aligned}$$

(in general, the limit values are different in these two cases).

Proof. In the following, we consider the expected value $h_{\exp}(\alpha)$ of the partition entropy in the region either to the left or to the right of the vertex of the asymmetric tent map. Within each interval, the slope of the map is constant, and the slope is $\alpha > 0$. In the right-hand section, although $\alpha < 0$, the same argument as the left-hand one is applied by treating the map as if it were inverted left and right, using i' numbered in the reverse order of that on the left-hand side. Let n be the number of intervals in the region. From Theorem 3, when α is an irrational

number, the expected value of partition entropy $h_{\exp}(\alpha)$ for $n \to \infty$ is as

$$\begin{aligned}
h_{\exp}(\alpha) &= \lim_{n\to\infty} \frac{1}{n} \sum_{i=1}^{n} h(i) \\
&= \lim_{n\to\infty} \frac{1}{n} \sum_{i=1}^{n} \Bigg(-\log \frac{1}{\alpha} - \frac{1}{\alpha} \langle i\alpha \rangle \log \langle i\alpha \rangle \\
&\quad - \frac{1}{\alpha} \{1 - \langle (i-1)\alpha \rangle\} \log \{1 - \langle (i-1)\alpha \rangle\} \Bigg), \\
&\quad \text{where } \langle i\alpha \rangle \text{ is replaced by } q \text{ and} \\
&= -\log \frac{1}{\alpha} + \frac{1}{\alpha} \int_0^1 (-q \log q)\, dq \\
&\quad + \frac{1}{\alpha} \int_0^1 (-(1-q) \log(1-q))\, dq \\
&= \log \alpha + \frac{1}{2\alpha}.
\end{aligned} \tag{2.3.18}$$

On the other hand, when α is a rational number, the expected value is as

$$\begin{aligned}
h_{\exp}(\alpha) &= \lim_{n\to\infty} \frac{1}{n} \sum_{i=1}^{n} h(i) \\
&= \lim_{n\to\infty} \frac{1}{n} \sum_{i=1}^{n} \Bigg(-\log \frac{1}{\alpha} - \frac{1}{\alpha} \langle i\alpha \rangle \log \langle i\alpha \rangle \\
&\quad - \frac{1}{\alpha} \{1 - \langle (i-1)\alpha \rangle\} \log \{1 - \langle (i-1)\alpha \rangle\} \Bigg) \\
&= \log \alpha + \frac{2}{m\alpha} \sum_{i=0}^{m-1} \left(-\frac{i}{m} \log \frac{i}{m} \right).
\end{aligned} \tag{2.3.19}$$

Since the slope of the left-hand side function $f_{L,a}(x)$ is $\alpha = a$ and that of the right-hand side function $f_{R,a}(x)$ is $\alpha = a/(a-1)$ (which is regarded as positive by reversing left and right), when a is an irrational number, the limit value of chaos degree for $N \to \infty$ is as

$$\begin{aligned}
&\lim_{N\to\infty} H_{CD} \\
&= \int_0^{\frac{1}{a}} h_{\exp}(a)\, \rho(x) dx + \int_{\frac{1}{a}}^1 h_{\exp}\left(\frac{a}{a-1} \right) \rho(x) dx \\
&= -\frac{1}{a} \log \frac{1}{a} - \frac{a-1}{a} \log \frac{a-1}{a} + \frac{1 + (a-1)^2}{2a^2}.
\end{aligned} \tag{2.3.20}$$

On the other hand, when a is a rational number $a = n/m$ (n and m are prime to each other), the limit value is as

$$\begin{aligned}
&\lim_{N\to\infty} H_{CD} \\
&= \int_0^{\frac{1}{a}} h_{\exp}(a)\,\rho(x)dx + \int_{\frac{1}{a}}^{1} h_{\exp}\left(\frac{a}{a-1}\right)\rho(x)dx \\
&= -\frac{m}{n}\log\frac{m}{n} - \frac{n-m}{n}\log\frac{n-m}{n} \\
&\quad + \frac{2m}{n^2}\sum_{i=0}^{m-1}\left(-\frac{i}{m}\log\frac{i}{m}\right) \\
&\quad + \frac{2(n-m)}{n^2}\sum_{i=0}^{n-m-1}\left(-\frac{i}{n-m}\log\frac{i}{n-m}\right).
\end{aligned} \tag{2.3.21}$$

□

Fig. 2.8 shows a plot of the limit values of chaos degree for the parameter a.

2.3.5 Discussion

As is clear from Fig. 2.8, the limit values of chaos degree with infinite number of partitions in asymmetric tent maps are generally very different for the cases where the parameter a is irrational and rational. This difference is due to the fact that the distribution of $\langle i\alpha\rangle$ differs between the continuous uniform distribution (when a is irrational) and the discrete uniform distribution (when a is rational) in Theorem 3.

The limit value of chaos degree is the sum of Lyapunov exponent and "other terms" in both cases where a is rational and irrational. The sum of first and second terms in the equations (2.3.20) and (2.3.21) is Lyapunov exponent, and the other terms are considered to be related to the partition used in the calculation of chaos degree (this interpretation is similar to the previous study [16]). It is in the terms other than Lyapunov exponent that the influence of the different distribution of $\langle i\alpha\rangle$ depending on whether the parameter a is rational or irrational becomes apparent.

When a is a rational number, terms of the influence of partition becomes smaller than in the case of an irrational number, and as a result, the limit value of chaos degree is closer to Lyapunov exponent. When a is represented by an irreducible fraction n/m, the number of elements of X, the set of possible values of $\langle i\alpha\rangle$, is m on the left and $n-m$ on the right. For very small values of m and $n-m$, the discrete uniform distribution of $\langle i\alpha\rangle$ deviates greatly from the continuous uniform distribution, and the limit value of chaos degree also differs greatly from

that when a is irrational. For example, $a = 2 = 2/1$ and $a = 3 = 3/1$ in Fig. 2.8 are remarkable. Conversely, the larger the value of m or $n - m$, the smaller the deviation of the distribution of $\langle i\alpha \rangle$ from the continuous uniform distribution, and the smaller difference of the limit value of chaos degree from the case when a is an irrational number. Furthermore, in the limit where m or $n - m$ is infinity, the limit value of chaos degree when a is a rational number equals that when a is an irrational number.

2.3.6 Conclusion

In this study, we analytically derived the limit value of chaos degree of asymmetric tent maps for infinite number of partitions and found that the limit values differ significantly depending on whether the parameter is rational or irrational. As shown in the results obtained in this study, chaos degree may include unexpected effects due to the nature of the mapping and partitioning. Therefore, quantitative evaluation of chaos using chaos degree should be done with caution even when the number of partitions is set sufficiently large.

The expected value of the partition entropy when the parameter is an irrational number is found to be $1/(2\alpha)$ added to the value equivalent to Lyapunov exponent, where α is the slope of the map. This result is consistent with the previous study [22] that examined chaos degree for logistic maps. In order to clarify whether the same argument can be applied to other general chaotic maps, it is left for future work to investigate the cause of the difference of $1/(2\alpha)$ between the partition entropy and Lyapunov exponent.

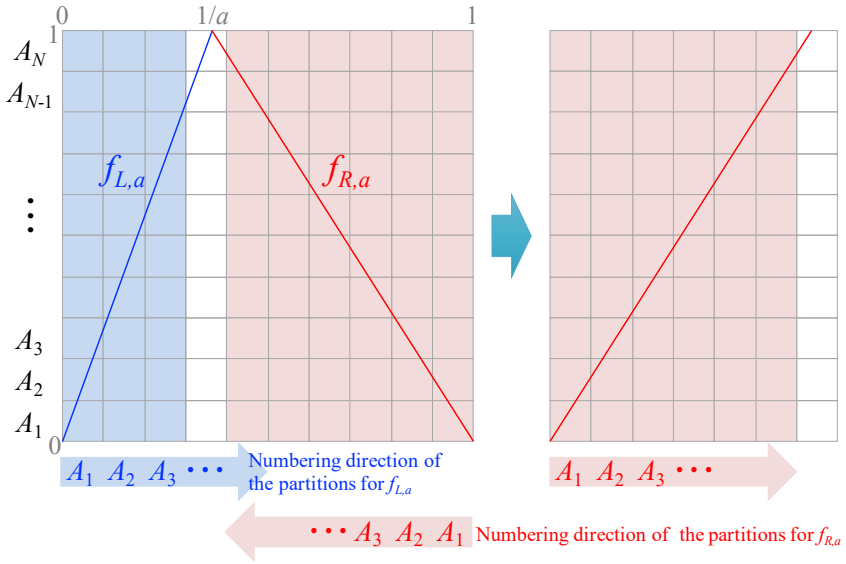

Figure 2.6: Example of asymmetric tent maps and partition, and the concept of right-side part numbering and inversion.

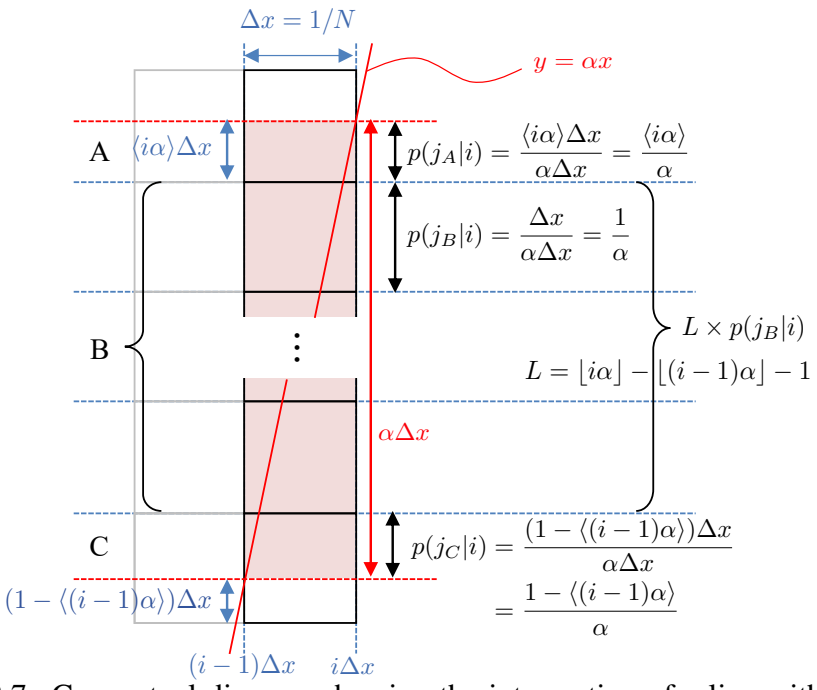

Figure 2.7: Conceptual diagram showing the intersection of a line with slope α ($y = \alpha x$) and equipartition at a certain interval A_i.

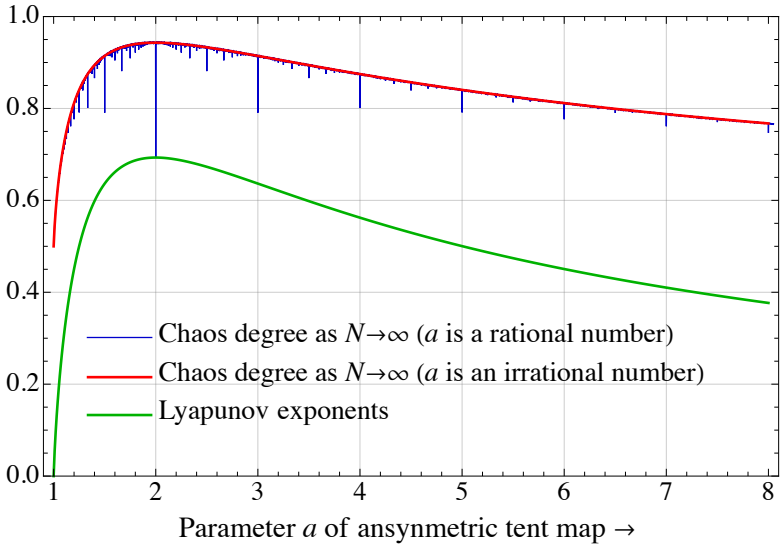

Figure 2.8: Plot of the limit values of chaos degree as the partition number $N \to \infty$ when the parameter a is an irrational and rational number and Lyapunov exponent against a.

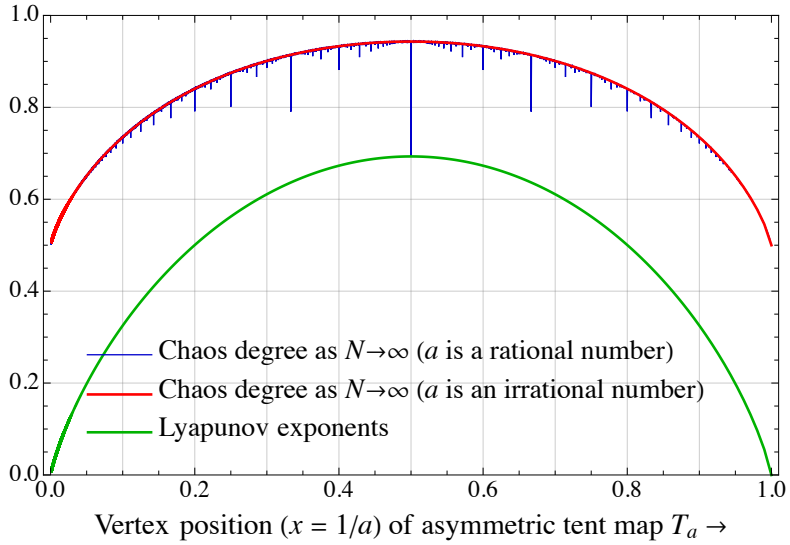

Figure 2.9: Plot of the limit values of chaos degree as the partition number $N \to \infty$ when the parameter a is an irrational and rational number and Lyapunov exponent against the coordinates $1/a$ of the vertex of asymmetric tent maps.

Chapter 3

Estimation of Lyapunov exponent by improved chaos degree

This chapter is according to the [23].

3.1 Introduction

Lyapunov exponent, that is a measure of sensitivity to initial conditions, is commonly used to quantify chaos. However, it is difficult to calculate Lyapunov exponent when the equations of the dynamical system are not given, such as when only time series data are available. As presented in [25] [26], typical methods for estimating Lyapunov exponents from time series data include the methods of Wolf *et al.*[12], Rosenstein *et al.*[13], and Kantz[14]. However, there are many issues in applying these methods to actual data analysis, such as the large amount of computation and data required for estimation and the need to appropriately determine parameters such as embedding dimension and time lag.

On the other hand, entropic chaos degree (hereafter simply called chaos degree) has been proposed from the viewpoint of information theory [15, 27]. Chaos degree is considered to be a quantitative measure of chaos equivalent to Lyapunov exponent. Chaos degree has the advantage that it can be computed only from obtained time series data, and is expected to have a wide range of applications. The relationship between chaos degree and Lyapunov exponent, particularly with respect to the magnitude relationship, has been discussed in previous studies such as [21], and [22] has showed analytically that the limit of chaos degree with infinite number of divisions is larger than Lyapunov exponent. Since the chaos measure is larger than Lyapunov exponent in many cases, it is necessary to be careful in judging chaoticity based on the positive value of chaos degree. For example, previous studies [19, 20] have shown that chaos degree is positive even when the

orbit is a quasiperiodic orbit, and it is difficult to distinguish it from a chaotic orbit.

3.2 Chaos degree

3.2.1 Definition of chaos degree

The definition of chaos degree in difference equations is as below [20].

We assume that the difference equation is determined by a map $f : I \to I$ ($\equiv [a, b]^d \subset \mathbf{R}^d,\ a, b \in \mathbf{R}, d \in \mathbf{N}$), i.e., $x_{n+1} = f(x_n)$ $(n = 0, 1, \ldots)$. Let x_0 be an initial value, and $A = \{A_i\}$ be a finit partition of I such that

$$I = \bigcup_{k=1}^{N} A_k,\ A_i \cap A_j = \emptyset\ \ (i \neq j). \tag{3.2.1}$$

The probability distribution $p_{i,A}^{(m)}(M)$ at the time m is given as

$$p_{i,A}^{(m)}(M) = \frac{\#\{x_k \in A_i;\ k = m, m+1, \ldots, m+M-1\}}{M}, \tag{3.2.2}$$

and the joint probability distribution $p_{i,j,A}^{(m,m+1)}(M)$ between the time m and $m+1$ is given as

$$p_{i,j,A}^{(m,m+1)}(M) = \frac{\#\left\{(x_k, x_{k+1}) \in A_i \times A_j;\ k = m, m+1, \ldots, m+M-1\right\}}{M}. \tag{3.2.3}$$

Then chaos degree $D^{(M,m)}(A, f)$ for the orbit $\{x_k\}$ is defined by

$$D^{(M,m)}(A, f) = \sum_{i=1}^{N}\sum_{j=1}^{N} p_{i,j,A}^{(m,m+1)}(M) \log \frac{p_{i,A}^{(m)}(M)}{p_{i,j,A}^{(m,m+1)}(M)}. \tag{3.2.4}$$

In this paper, we simplify $p_{i,A}^{(m)}(M) = p(i)$ and $p_{i,j,A}^{(m,m+1)}(M) = p(i, j)$, then chaos degree H_{CD} is calculated as:

$$H_{CD} = \sum_{i=1}^{N}\sum_{j=1}^{N} p(i, j) \log \frac{p(i)}{p(i, j)} \tag{3.2.5}$$

$$= -\sum_{i=1}^{N} p(i) \sum_{j=1}^{N} p(j|i) \log p(j|i), \tag{3.2.6}$$

where the conditional probability $p(j|i) = \dfrac{p(i, j)}{p(i)}$.

3.2.2 Relationship between chaos degree and Lyapunov exponent

The previous study [22] shows analytically that the limit of chaos degree with infinite number of divisions (the width of the interval of divisions $\Delta x \to 0$ and considered as the limit of the Riemann sum) is Lyapunov exponent with a non-negative function $D(x)$ added to the integrand, that is,

$$\lim_{\substack{\Delta x \to 0 \\ N \to \infty}} H_{CD} = \int_I (\log |f'(x)| + D(x))\, \rho(x) dx. \tag{3.2.7}$$

It can be inferred that the limit of chaos degree is the Lyapunov exponent with some additional information, but the function $D(x)$ in the limit with infinite number of partitions is indefinite and cannot be expressed explicitly. The discussion in below is limited to a finite number of divisions.

In the previous study [16], we investigated the difference between chaos degree and Lyapunov exponent for asymmetric tent maps, and showed that the difference can be interpreted as an average of the information amount. In this paper, we extend this to other one-dimensional mappings and propose improved chaos degree that subtracts the information amount of the difference from chaos degree.

3.3 Improved chaos degree

3.3.1 Assumptions

In discussing the relationship between chaos degree and Lyapunov exponent in this chapter, we make the following assumptions. We deal with a one-dimensional map f that has an invariant measure $\rho(x)$ absolutely continuous with respect to Lebesgue measure. The partitions used to compute chaos degree are equally spaced, and each interval is assumed to be uniformly enlarged or reduced by f (Fig. 3.1). That is, the number of divisions is assumed to be sufficiently large so that f can be regarded as a line in each interval.

The expansion rate of the interval A_i is

$$r(i) = \frac{\|f(A_i)\|}{\|A_i\|}. \tag{3.3.1}$$

If the expansion rate is less than 1, it means contraction. In this paper, we consider the case where $r(i) \neq 0$, i.e., $r(i) > 0$, for all segments. The conditional probability is as

$$p(j|i) = \frac{\|f(A_i) \cap A_j\|}{\|f(A_i)\|}. \tag{3.3.2}$$

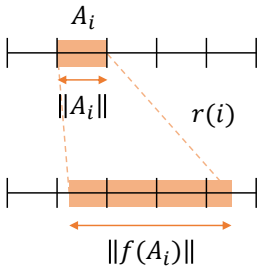

Figure 3.1: Schematic picture of mapping.

In addition, let $\{A_i\}$ be an equipartition. Therefore,

$$\|A_i\| = \|A_j\|. \tag{3.3.3}$$

3.3.2 Cases of difference between the chaos degree and Lyapunov exponent

In the following, we will use Fig. 3.2 to illustrate when the difference between chaos degree and Lyapunov exponent occurs in the calculation of the chaos degree. Case (a) is the case where the expansion rate of the interval is 1 and the mapped destination region is exactly one interval. Case (b) is the case where the expansion rate of the interval is 1, but the mapped destination region spans two intervals equally. Case (c) is the case where the expansion rate of the interval is 2 and the mapped destination region is exactly two intervals.

In each case, the entropy of the conditional probability, $s = -\sum_j p(j|i) \log p(j|i)$, is calculated to be $s = 0$ in (a) and $s = \log 2$ in (b) and (c). Comparing (a) and (b), the values of entropy of conditional probability are different only due to the difference in the positional relationship with the partition, even though the expansion rate is the same 1 in both cases. Comparing (b) and (c), the conditional probabilities and their entropies are the same in both cases, even though the expansion rate is different. In case (b), the two mapped intervals are not mapped to the whole intervals, but only to one half of the intervals. However, since the conditional probability is not affected whether the mapped region is the entire interval or only a part of the interval, the entropy s is exactly the same as when the entire interval is mapped (i.e., case (c)).

Therefore, the value of the entropy of the conditional probability (and hence chaos degree) calculated in a case like (b) does not evaluate only the information generated by the expansion of the mapping, but also the amount of information determined by the positional relationship between the mapped region and the partition.

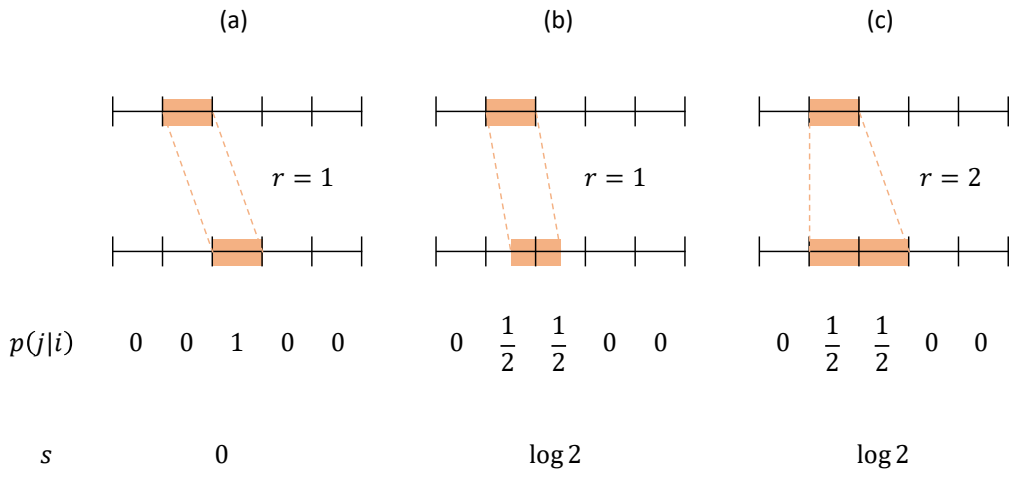

Figure 3.2: Example of a case that there is a difference between chaos degree and Lyapunov exponent for an expansive mapping.

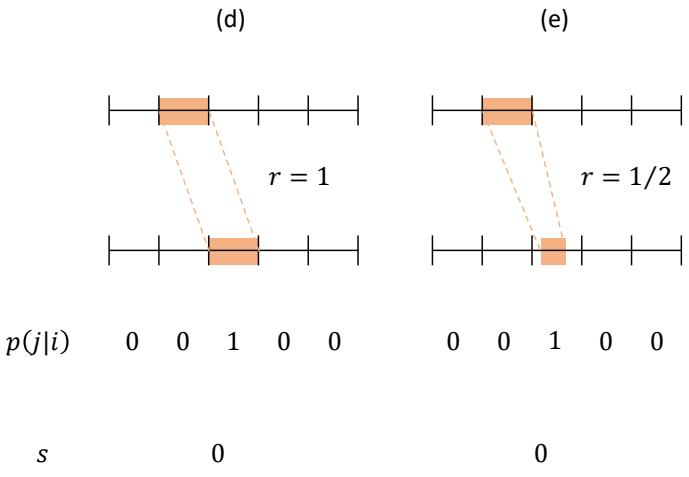

Figure 3.3: Example of a case that there is a difference between chaos degree and Lyapunov exponent for a contraction mapping.

Next, we illustrate the case where the mapping is contractional (Fig. 3.3). Case (d) is the case where the expansion rate of the interval is 1 and the mapped destination region is exactly one interval. Case (e) is the case where the expansion rate of the interval is 1/2 and the mapped destination region is within one interval.

In the case (e), the conditional entropy cannot be less than zero, although the effect on the Lyapunov exponent of the interval is negative. In such case, chaos degree is evaluated as a larger value than Lyapunov exponent.

3.3.3 Improved chaos degree

When an interval A_i is mapped to $f(A_i)$ by a mapping f, as in the example shown in the previous section, the entropy of the conditional probability is the same as when $f(A_i)$ is mapped over the entire interval A_j, even if $f(A_i)$ intersects only a part of the interval A_j. That is, chaos degree in such a case is considered to be evaluated as a value larger than Lyapunov exponent.

Therefore, we evaluate the difference between chaos degree and Lyapunov exponent as the amount of information, and define a new chaos degree by subtracting the amount of information from chaos degree.

First, let $q(i, j)$ be defined as the ratio of the interval A_j that is occupied by the region where the interval A_i is mapped by the mapping f, i.e.,

$$q(i, j) = \frac{\|f(A_i) \cap A_j\|}{\|A_j\|}. \tag{3.3.4}$$

In the previous study [16], the information amount due to this $q(i, j)$, i.e.

$$-\log q(i, j) \tag{3.3.5}$$

is suggested to be the reason for the difference between chaos degree and Lyapunov exponent in asymmetric tent maps.

Intuitively, this can be interpreted as follows. When an interval A_i is mapped by a mapping f, how the output $f(A_i)$ is distributed in A_j does not affect the calculation of chaos degree. Then, chaos degree is the same value as if $f(A_i)$ were uniformly distributed over the entire interval A_j. However, since the region where $f(A_i)$ is distributed in the interval A_j is actually limited to $f(A_i) \cap A_j$, a larger value of entropy is calculated with respect to the expansion rate of the mapping. The entropy overestimated in this case is considered to be $-\log q(i, j)$, the amount of information required to narrow down the region where output values of the mapping f are distributed from the entire interval A_j to $f(A_i) \cap A_j$.

The average of this amount of information is subtracted from the calculation

of chaos degree, i.e.

$$\tilde{H}_{CD} = \sum_{i=1}^{N} p(i) \sum_{j=1}^{N} p(j|i) \{-\log p(j|i) - (-\log q(i,j))\} \tag{3.3.6}$$

is defined as a new chaos degree (improved chaos measure). If we rearrange the equation (3.3.6) as

$$\tilde{H}_{CD} = \sum_{i=1}^{N} p(i) \sum_{j=1}^{N} p(j|i) \log \frac{q(i,j)}{p(j|i)}, \tag{3.3.7}$$

improved chaos degree can be interpreted as chaos degree redefined using a new information measure $\log \frac{q(i,j)}{p(j|i)}$.

3.3.4 Theorem and proof

The following theorem holds for improved chaos degree defined in the previous section.

Theorem 5. *Let f be a one-dimensional map with an invariant measure that is absolutely continuous with respect to Lebesgue measure. Let $\{A_i\}$ be an N-equipartition of the domain I of f, where each interval A_i is uniformly expanded by f with expansion rate $r(i)$. Improved chaos degree is equivalent to the approximation obtained by replacing the spatial integration using the invariant measure $\rho(x)$ of f of the definition of Lyapunov exponent $\lambda = \int \log |f'(x)| \rho(x) dx$ with the sum with partition $\{A_i\}$. Note that let f be regarded as a line in each partition and $|f'(x)| = r(i)$ be constant in each partition.*

Proof. From equations (3.3.1) (3.3.2) (3.3.3) (3.3.4), the part of the definition formula for improved chaos degree (3.3.6) that is the sum with respect to j is as

$$\sum_{j} p(j|i) \{-\log p(j|i) - (-\log q(i,j))\} \tag{3.3.8}$$

$$= \sum_{j} p(j|i) \left\{ -\log \frac{\|f(A_i) \cap A_j\|}{r(i)\|A_i\|} - \left(-\log \frac{\|f(A_i) \cap A_j\|}{\|A_j\|} \right) \right\} \tag{3.3.9}$$

($\because$ From equation (3.3.1), $\|f(A_i)\| = r(i)\|A_i\|$ is applied to equation (3.3.2))

$$= \sum_{j} p(j|i) \left(\log \frac{r(i)\|A_i\|}{\|A_j\|} \right) \tag{3.3.10}$$

$$= \sum_{j} p(j|i) \log r(i) \tag{3.3.11}$$

$$= \log r(i). \tag{3.3.12}$$

Thus, improved chaos degree is as

$$\tilde{H}_{CD} = \sum_i p(i) \log r(i). \tag{3.3.13}$$

Here, $r(i) \to |f'(x)|$ and $p(i) \to \rho(x)dx$ in $N \to \infty$, therefore the limit of $\tilde{H}_{CD}$ for $N \to \infty$ is

$$\lim_{N\to\infty} \tilde{H}_{CD} = \int_I \log |f'(x)| \rho(x) dx. \tag{3.3.14}$$

Because the right-hand side is the Lyapunov exponent itself, the improved chaos degree $\tilde{H}_{CD}$ is none other than the Lyapunov exponent discretized with the partition $\{A_i\}$. □

3.4 Numerical experiment

3.4.1 Experiment 1

To confirm the usefulness of improved chaos degree, we conducted a numerical experiment to compare it with conventional chaos degree and Lyapunov exponent. The experiment included logistic map

$$f(x) = ax(1 - x). \tag{3.4.1}$$

The parameter a was varied from 3.5 to 4.0, and for each parameter, a series $\{x_n\}$ of length 10000000 was generated with initial values $x_0 = 0.01$ and $x_{n+1} = f(x_n)$. The Lyapunov index, chaos degree by conventional definition, and improved chaos degree were calculated.

The conventional chaos degree was calculated based on the definition equation (3.2.6). The number of partition N is set to 100. Improved chaos degree was calculated based on the definition equation (3.3.6). The number of partition N is set to 100. However, $q(i, j)$ in the definition is determined by mapping and partitioning, and cannot be obtained directly from the data, but its approximation is obtained by the following procedure. The interval A_j is divided into Q subdivisions $B_l (l = 1, 2, \ldots, Q)$ at equal intervals, the number L of subdivisions B_l such that $x_k \in A_i$ and $x_{k+1} \in B_l$ is counted, and the ratio L/Q is regarded as the approximation value of $q(i, j)$. The number of subdivisions Q is set to 100.

3.4.2 Result 1

The result of experiment 1 is shown in Fig. 3.4.

Improved chaos degree is found to be close to the Lyapunov exponent, especially in the regions where the Lyapunov exponent is positive. In regions where

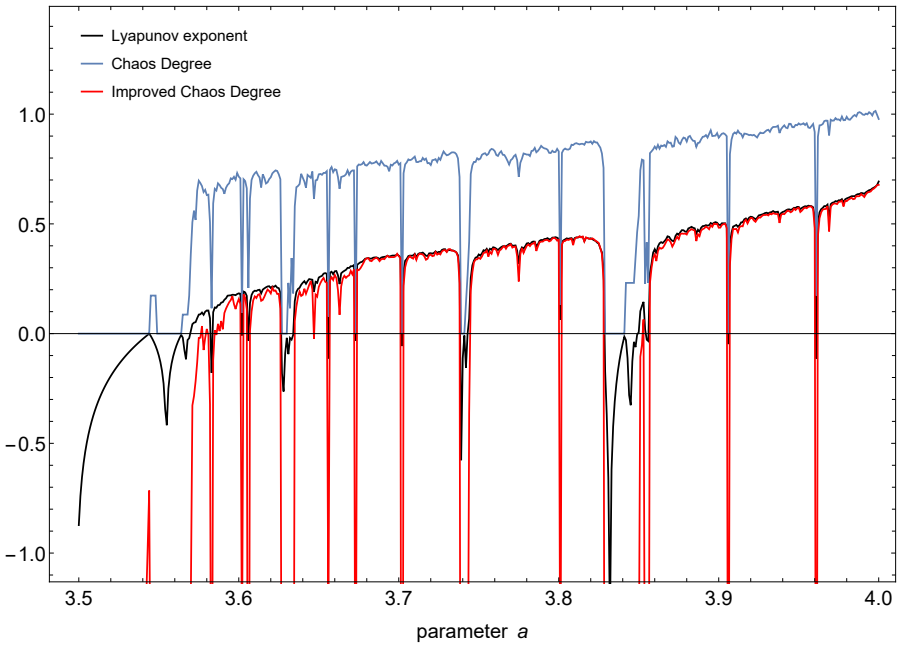

Figure 3.4: Comparison among Lyapunov exponent (black), chaos degree (blue) and improved chaos degree (red) for parameter a of logistic map $f(x) = ax(1-x)$.

the Lyapunov exponent is negative, the values of improved chaos degree are also clearly negative. In such regions, the orbits are periodic, and each interval is mapped to only one point (thus expansion rate of the interval $r(i) = 0$). In this case, the term $-(-\log q(i,j))$ in the definition of improved chaos degree (3.3.6) diverges to $-\infty$. In practice, improved chaos degree takes finite values due to the finite number of subdivisions B_l, but improved chaos degree results in a smaller value than the true Lyapunov exponent.

This result suggests that a positive or negative value of improved chaos degree calculated from the data sequence alone may provide a judgment equivalent to that of Lyapunov exponent, although care must be taken when the orbit is periodic.

3.4.3 Experiment 2

In Experiment 1, improved chaos degree is found to be closer to Lyapunov exponent than chaos degree with the conventional definition. However, in the calculation of improved chaos degree, each segment is further subdivided into smaller segments to estimate $q(i,j)$, thus the comparison between improved chaos degree and the conventional chaos degree in Experiment 1 may not be a fair comparison in terms of the fineness of the division.

Therefore, we conducted Experiment 2 below to compare improved chaos degree with the conventional chaos degree under the condition that the number of divisions is equivalent in real terms. As in Experiment 1, logistic map is used, and the parameter a is varied from 3.5 to 4.0.

First, we compute chaos degree using the conventional definition, where the number of partition N is 20. Let this be condition (1). Next, we compute chaos degree by the conventional definition, where the number of partition N is 400, which is 20 times larger than condition (1). Let this be condition (2). Furthermore, we compute improved chaos degree in which the number of divisions N is set to 20 and $q(i, j)$ is estimated by subdividing each interval into 20, so that the actual number of divisions is 400, which is equivalent to condition (2). This is condition (3). The values of chaos degree are computed and compared for each of the above conditions (1) to (3).

3.4.4 Result 2

The result of experiment 2 is shown in Fig. 3.5.

Note that the black line in the figure is Lyapunov exponent, and the blue, green, and red lines are

blue line: conventional chaos degree according to condition (1),

green line: conventional chaos degree according to condition (2),

red line: improved chaos degree according to condition (3).

Even if the number of partition is increased by a factor of 20 from condition (1) to condition (2), the value of chaos degree (green line) is not necessarily close to Lyapunov exponent, but improved chaos degree (red line) for condition (3) with practically the same number of partition as condition (2) is close to Lyapunov exponent (black line).

From the above results, it can be inferred that the reason why improved chaos degree becomes close to the Lyapunov exponent is not due to the substantial increase in the number of partition, but because the difference between chaos degree and Lyapunov exponent is appropriately evaluated by the information amount $-\log q(i, j)$.

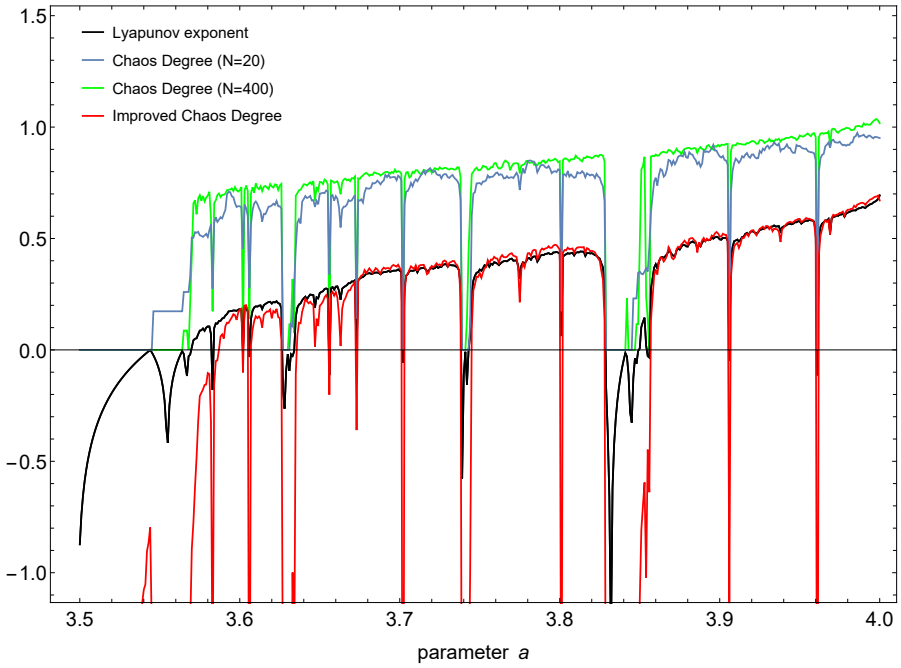

Figure 3.5: Comparison among Lyapunov exponent (black), chaos degree for $N = 20$ (blue), chaos degree for $N = 400$ (green) and improved chaos degree (red) for parameter a of logistic map $f(x) = ax(1 - x)$.

3.5 Comparison of the computational performance of improved chaos degree and SampEn

3.5.1 Computational performance of improved chaos degree

Another advantage of improved chaos degree is its low computational complexity. In order to evaluate the computational performance of improved chaos degree, we choose Rosenstein's method[13] and SampEn[28, 29] for comparison. Rosenstein's method is an algorithm for obtaining an estimate of the Lyapunov exponent from a data series. SampEn is increasingly being used as a measure to quantify the complexity of heart rate variability.

3.5.2 Methods of comparison

Using the logistic map f described in equation (3.4.1), the parameter a was varied from 3.5 to 4.0 in increments of 0.001, and for each a, a series of length $n = 3000$ was generated with initial value $x_0 = 0.01$, $x_{n+1} = f(x_n)$, and improved chaos degree, Lyapunov exponent by Rosenstein's method, and SampEn were calculated. The number of divisions N and the number of subdivisions Q for improved chaos degree were set to $N = 20$, $Q = 20$. In Rosenstein's method, lag $J = 1$ and embedding dimension $m = 2$. The parameters for SampEn were the commonly used $m = 2$, $r = 0.2\sigma$, where σ is the standard deviation of data series. Calculations were performed using Wolfram Mathematica 11.3 on iMac Pro (2017), CPU: 3.0GHz Intel Xeon W, RAM: 128GB.

3.5.3 Results

Results are shown in Fig. 3.6 and Table 3.1. Fig. 3.6 shows that the improved chaos degree, Rosenstein's method, and SampEn all capture the characteristics of chaos as well as the Lyapunov exponent. As shown in Table 3.1, the calculation took 75.9353 seconds for improved chaos degree, 10498.1 seconds for Rosenstein's method, and 83437.0 seconds for SampEn, which was by far the less time required to calculate improved chaos degree.

3.5.4 Discussion

To illustrate the difference in computation time between improved chaos degree, Rosenstein's method, and SampEn, a rough estimate of the computational complexity is given below. The number of calculations in the major for loop in the calculation of improved chaos degree depends on the number of divisions N

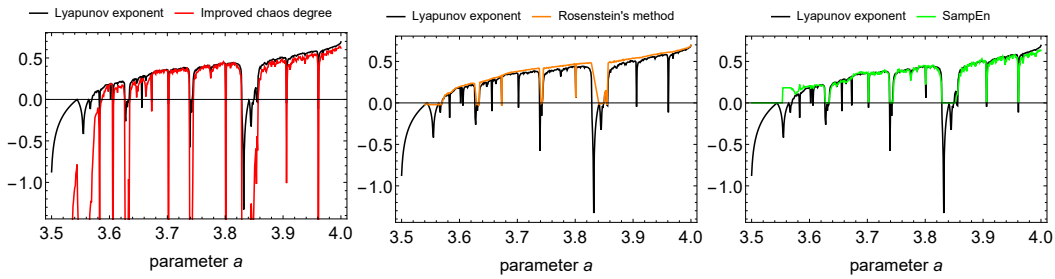

(a) Improved chaos degree

(b) Rosenstein's method

(c) SampEn

Figure 3.6: Figure showing the results of calculating (a) improved chaos degree, (b) Lyapunov exponent by Rosenstein's method, and (c) SampEn for the logistic map, plotted along with Lyapunov exponent.

Table 3.1: Comparison of computation time of improved chaos degree, Rosenstein's method, and SampEn for logistic map $f(x) = ax(1-x)$.

	Improved chaos degree	Rosenstein's method	SampEn
computation time [sec]	75.9353	10498.1	83437.0

and the number of subdivisions Q, thus the computational complexity is $O(N^2Q)$. On the other hand, the number of calculations in the major for loop in the calculation of Rosenstein's method or SampEn depends on the data length n, thus the computational complexity is $O(n^2)$. Here, the number of divisions N of improved chaos degree is generally $N < n^{\frac{1}{2}}$. This is because when $N > n^{\frac{1}{2}}$, the number of combinations of i and j in obtaining the conditional probability $p(j|i)$ becomes larger than the data length n, and there will be combinations of i and j for which $p(j|i) = 0$, regardless of the nature of the data. In such cases, it is hard to say that improved chaos degree accurately evaluates the chaotic nature of the data. Furthermore, if N and Q are also set to the same magnitude, then

$$O(N^2Q) \sim O(N^3) < O(n^{\frac{3}{2}}) < O(n^2). \tag{3.5.1}$$

Therefore, the computational complexity of improved chaos degree is smaller than that of Rosenstein's method or SampEn.

For reference, in this verification, $N^2Q = 20 * 20 * 20 = 8000$ and $n^2 =$

$3000 * 3000 = 9000000$. In this case, it can be confirmed that the relationship shown in equation (3.5.1) still holds.

These results confirm that improved chaos degree is significantly less computationally intensive than Rosenstein's method and SampEn. This means that improved chaos degree has a great advantage in applications.

3.6 Conclusion

In this paper, the difference between chaos degree and Lyapunov exponent is evaluated in terms of the amount of information and subtracted to define improved chaos degree. Theorems and numerical experiments show that improved chaos degree is equivalent to Lyapunov exponent. Improved chaos degree proposed in this paper may be able to compute a value close to Lyapunov exponent from data only. Improved chaos degree has the potential to be used for a wide variety of data analysis in addition to the determination of chaos.

Although only one-dimensional mapping was discussed in this chapter, improved chaos degree has been extended to multidimensional mapping [30]. That is, by applying the same idea to the case of multidimensional mapping as to the case of one-dimensional mapping described in this chapter, it is proved that the chaos degree extended to multiple dimensions is equal to the sum of Lyapunov exponents.

Furthermore, a comparison was made between improved chaos degree and SampEn in terms of computational complexity. The computational complexity of improved chaos degree was much smaller than that of SampEn, suggesting that improved chaos degree is useful for real-time data analysis.

Chapter 4

Hypotheses on chaos in heart rate variability

This chapter is according to [31].

4.1 Introduction

Heart rate variability in a healthy state is characterized by chaotic and complex fluctuations, while in a pathological state the variability loses its nonlinearity and becomes less variable and extremely predictable [32, 33]. What brings about chaos in heart rate variability, and what does it mean to measure chaos in HRV? There are no clear answers to these questions. In this chapter, to approach the answer to these essential questions, we hypothesize that the chaotic nature of HRV reflects brain network activity, based on findings from previous studies.

4.2 Limitations of conventional linear analysis of heart rate variability and expectations for chaos analysis

The autonomic nervous system is deeply involved in the control of the heartbeat, and it is known that the sympathetic nervous system accelerates the heartbeat and that the parasympathetic nervous system slows it. As a result, ”fluctuation” is induced in the RRI, and this phenomenon is called heart rate variability (HRV). We can evaluate the state of autonomic nervous system activity using the HRV analysis method standardized in 1996[3]. The HRV analysis method mainly consisted of the time-domain analysis (statistical analysis) and the frequency-domain analysis

(spectrum analysis).

However, time-domain and frequency-domain analysis captures only a part of the aspect of HRV. In other words, there exist aspects that are not clearly visible in conventional analysis, such as components that look like noise rather than periodic. This is clear, at least from a mathematical point of view. In Fig. 4.1, it is shown that the chaotic/complexity indices are independent of the time-domain indices of the conventional analysis. Therefore, the characterization of HRV by conventional indicators is limited, and identifying, for example, signs of disease or sudden death remains a major challenge[9].

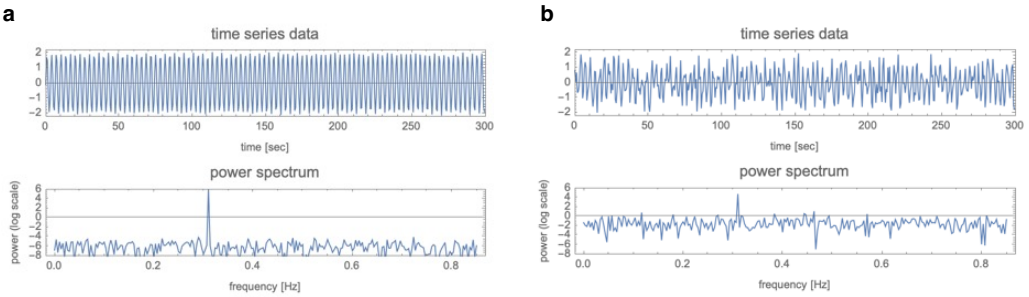

c

		a		b
time-domain analysis	SDNN	1.416	>	0.919
	SDSD	1.530	>	1.118
	RMSSD	1.530	>	1.118
chaotic/complexity analysis	CD	1.286	<	2.067
	ICD	1.016	<	1.773
	ApEn	0.140	<	1.356
	SampEn	0.155	<	2.068

Figure 4.1: Independence of chaotic/complexity analysis and conventional time-domain analysis[3]. **(a)** A highly periodic wave generated by adding random numbers uniformly distributed in the interval $[-0.1, 0.1]$ to a sine wave with a frequency of 0.31 [Hz] and an amplitude of 2. **(b)** A highly irregular wave generated by adding random numbers uniformly distributed in the interval $[-1, 1]$ to a sine wave with a frequency of 0.31 [Hz] and an amplitude of 1. **(c)** SDNN, SDSD, RMSSD, CD, ICD, ApEn, SampEn of two time series data shown in (a) (b). Since time series data (a) is larger in amplitude and more periodic (less complex) than (b), SDNN, SDSD, and RMSSD take large values, while CD, ICD, ApEn, and SampEn are small. Conversely, time series data (b) has smaller amplitude and lower periodicity (higher complexity) than (a), so SDNN, SDSD, and RMSSD take small values, while CD, ICD, ApEn, and SampEn take large values. In other words, the chaos/complexity analysis indices (CD, ICD, ApEn, and SampEn) are independent of the time-domain analysis indices (SDNN, SDSD, and RMSSD) of the conventional analysis[3].

On the other hand, since the human body, especially the circulatory system, is supposed to be a typical nonlinear system, the development of nonlinear analysis methods and research to understand their meanings are expected. That is, measuring the chaos/complexity of HRV may extract new information on the heart rate generation mechanism contained in HRV from a different perspective than conventional methods. A nonlinear approach is appropriate to describe complex phenomena such as HRV[4, 34]. Chaos is known as the property through which even a simple and deterministic system can produce complex results[35, 36]. It has been suggested that there may be chaotic dynamics in HRV[37, 38]. However, there is still no clear explanation for how the chaos of HRV occurs in relation to the specific mechanism of heart rate generation. Therefore, it is unclear what can be quantified by measuring the chaos or complexity of HRV, and the chaos/complexity indices has not been clinically utilized.

4.3 Review of previous studies on brain activity and heart rate variability

There are some interesting studies that experimentally investigated the relationship between brain activity (cognition, mood, anxiety, stress, etc.) and HRV. These previous studies often used time-domain analysis and frequency-domain analysis of the RRI; these approached have been conventionally used in the field of autonomic nervous system evaluation. Recently, complexity analysis has also come to be used. In experiments using frequency-domain analysis, it was reported that the index of power in high frequency range (HF) decreased with physical stress and mental stress, but the amount of decrease was small under mental stress, and the ratio of power in low frequency range to power in high frequency range (LF/HF) was significantly larger under physical stress[39].

In experiments using complexity analysis, it was reported that the conditional entropy of blood pressure and respiration increased during mental arithmetic, but there was no significant difference in the conditional entropy of the RRI[5]. On the other hand, RRI entropy has been reported to increase when individuals are performing cognitive tasks without stressors, which are external factors, such as noise, that impede concentration during cognitive task performance[6]. It has also been reported that individuals who exhibit an anxiety response have significantly reduced HRV complexity when in a state of anxiety or stress compared to that of individuals who do not exhibit an anxiety response[7]. It has also been reported that heart rate complexity may be more closely related to cognition and mood than time-domain and frequency-domain indicators[8].

These previous studies have shown slightly different conclusions because the

purpose and conditions of each experiment were slightly different and because the same analytical method was not used in all experiments. Furthermore, there is still no clear explanation of what the chaos/complexity of HRV implies.

4.4 Review of previous studies on NVI model and brain network

In the following, we consider the mechanism by which brain activity increases the chaotic/complexity of HRV. Previously, the center of the autonomic nervous system was thought to be the hypothalamus. A recent study in brain science revealed that the center of the autonomic nervous system is a network in the brain called the central autonomic network (CAN), which consists of the hypothalamus, anterior cingulate gyrus, insular cortex, and amygdala[40]. In addition, the neurovisceral integration (NVI) model[41], which explains the pathway by which activation of the prefrontal cortex connected to the CAN affects heartbeat regulation via autonomic nerves, and the extended model from the viewpoint of functional and neuroanatomy (8-layer model)[42] have been proposed. That is, these models[41, 42] suggest that HRV is affected by higher-order brain function.

Brain and chaos are closely related. The electroencephalogram (EEG) of the olfactory system due to chaotic brain activity has been explained by animal experiments and mathematical model simulations [43, 44]. It has been suggested that chaotic itinerancy in neural activity play an important role in memory mechanisms [45]. Considering the NVI model described above, it is natural to assume that chaotic brain activity influences HRV.

To consider the effect of brain activity on the chaotic nature of HRV, the activity and connectivity of large-scale brain networks during cognitive tasks in previous studies could be summarized as follows. It is known that the default mode network (DMN) is deactivated during cognitive tasks by task-induced deactivation caused by resource reallocation[46]. Recent studies have reported that the DMN and executive control network (ECN) cooperate depending on the character of the task[47]. The ECN is also expressed as the central executive network (CEN). The salience network (SN) is involved in switching and adjusting the DMN and ECN[48, 49]. Also, it is considered that the ECN, DMN, and SN operate during cognitive tasks while maintaining functional independence and being connected to each other. On the other hand, it has been reported that functional connectivity analysis of functional magnetic resonance imaging (fMRI) data confirmed that the connectivity between the DMN and SN increased and the connectivity between the DMN and ECN decreased during cognitive tasks with stressors[50, 51]. The association of heart rate variability with brain network activity after acute stress

has been suggested by [52].

4.5 Extended Neurovisceral Integration Model and Hypothesis

Here, we synthesize the above review and propose a hypothesis and a model that explain the effect of the activity and connectivity of brain networks on the chaoticity of HRV(Fig. 4.3).

- Hypothesis : The complexity of the behavior of the DMN, ECN, and SN, which are the three major brain networks that interact with each other, causes chaos in HRV.

- Explanation : The behavior of the three brain networks is similar to the three-body system creating a complicated orbit due to their chaotic nature, even if their interactions are simple, as is the case with gravity.

The behavior of the three networks becomes complicated, and the HRV becomes chaotic if the networks with similar activity and connectivity interact with each other. On the other hand, imbalances in activity and/or connectivity reduce the degree of freedom of the three networks and decrease the chaos of HRV. The proposed hypothetical model can explain that the significant increase in the chaos indices of HRV in the Brain Task states in this experiment is because the operation of all three networks became complicated by reducing the imbalance in the activity magnitude of each network. In addition, this model could explain that the experimental result[6] that the complexity index of HRV decreased during the cognitive task with stressors is due to the decrease in the degree of freedom of the three networks by the increase in DMN-SN connectivity.

4.6 Conclusion

In this chapter, we hypothesize that the chaotic nature of heart rate variability arises from chaotic interactions similar to the three-body problem in major brain networks. Although this hypothesis is a simple one, we hope that it will provide a basis for explaining the relationship between brain and heart.

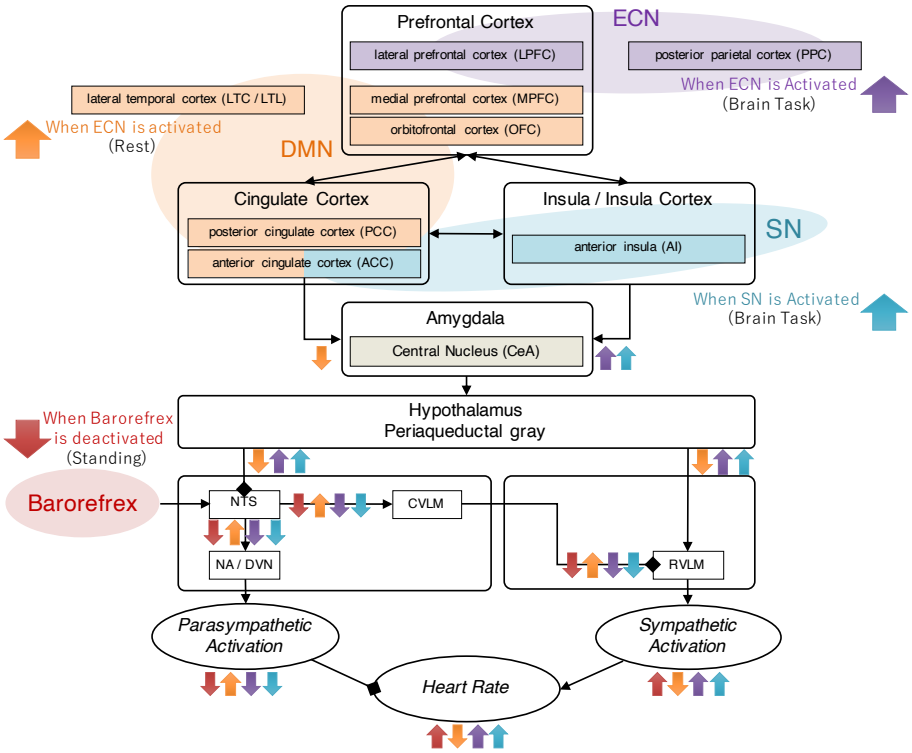

Figure 4.2: Expanded neurovisceral integration model based on previous results of large-scale brain networks and fMRI studies. The extended neurovisceral integration model describes that DMN activation (Rest) leads to deactivation of sympathetic nerve activity and activation of parasympathetic nerve activity, and conversely, ECN activation and SN activation (Brain Task) leads to activation of sympathetic nerve activity and deactivation of parasympathetic nerve activity. However, in this experiment, the above-mentioned activation or deactivation of autonomic nerve activity could not be significantly captured by the conventional HRV analysis (autonomic nerve analysis). Therefore, the reason for chaotic HRV is presumed to be due to a mechanism other than the simple activation / deactivation of the autonomic nervous system.

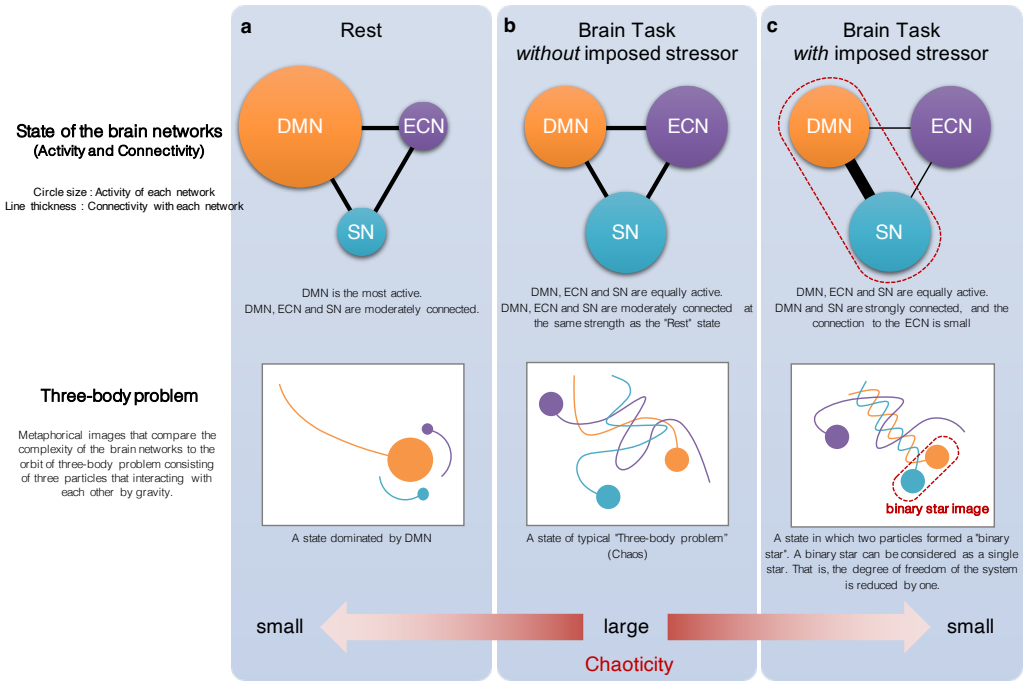

Figure 4.3: A model that explains that higher-order brain function brings chaos to HRV. **(a)** In the Rest state, the default mode network (DMN) is the most active. In addition, the DMN, executive control network (ECN) and salience network (SN) are moderately connected. Therefore, since the activity of the higher-order brain system, which consists of the DMN, ECN and SN, is controlled by one strong mode (DMN), the chaoticity in the system is small or does not appear. **(b)** In the Brain Task without imposed stressor, the DMN, ECN and SN are equally active. In addition, the DMN, ECN and SN are connected at the same strength as the Rest state. That is, the higher-order brain system has three equal powered modes and is in a state of antagonism. In this case, the strong chaos may be caused in the system. According to the neurovisceral integration model, it can be explained that the chaos caused in the higher-order brain system brings chaos in autonomic nervous system, and finally, HRV becomes chaotic. **(c)** In the Brain Task with imposed stressor, the DMN, ECN and SN are equally active. However, the DMN and SN are strongly connected, and the connection to the ECN is weak. Therefore, the activity of the higher-order brain system is biased towards the DMN and SN, which are strongly connected. Then, the chaoticity in the system is smaller than that in the Brain Task without imposed stressor state.

Chapter 5

Experimental verification

This chapter is according to [31].

5.1 Introduction

In the previous chapter, we hypothesized that the chaos of heart rate variability reflects the complexity of brain network activity. In this chapter, as a first step to experimentally verify this hypothesis, we clarify the link between brain activity and heart rate variability by measuring chaos indices.

The association between brain network activity and heart rate variability has been suggested by [52]. However, as described in [52] as a limitation, only the time-domain index of heart rate variability, RMSSD, was observed. In our experiment, we experimentally show the relationship between brain network activity and heart rate variability using a set of nonlinear measures of chaos and complexity in addition to conventional time-domain and frequency-domain measures.

Although many previous studies have attempted to characterize heart rate variability in abnormal conditions such as disease, disorder, or high stress, few studies have examined normal conditions. We believe that it is important to first elucidate the mechanism by which brain activity affects the heart under normal conditions, thus we compared three conditions: resting state, cognitive task, and physical load (without cognitive activity) in the experiment.

5.2 Methods

5.2.1 Participants

This experiment was conducted with 18 healthy participants. There were 13 participants in their 20 s, 2 in their 30 s, and 3 in their 50 s; also, 15 were

males and 3 were females. This experiment was approved by the Research Ethics Committee of the Graduate School of Informatics, Kyoto University (the approval number: KUIS-EAR-2019-006) and was conducted according to the principles of the Declaration of Helsinki. Informed consent was obtained from all participants of the study. Informed consent was obtained for publication of the identifiable images from the relevant subject.

5.2.2 RRI measurement

The participants wore the Polar H10 chest strap heart rate sensor that can measure RRI and completed in two experiments in which their RRIs were measured under the following states.

- **Rest :** Sit in a chair and stay at rest under neither a physical nor mental load (Fig. 5.1(b-1)).

- **Standing :** Maintain an upright posture without leaning against a wall, desk, etc, and only a physical load is applied (Fig. 5.1(b-2)).

- **Brain Task :** Perform cognitive tasks (mental arithmetic or Sudoku) sitting in a chair and only a mental load is applied (Fig. 5.1(b-3)).

For the cognitive tasks in this experiment, participants were instructed in advance only to continue solving problems throughout the measurement, with no demands on their progress or performance on the task. During the execution of the task, the operator did not look in on the participant or check the progress of the task with the participant. Thus, this experiment did not impose any social mental stress on the subjects as described in [6, 52].

In Experiment 1, mental arithmetic (Fig. 5.1(c)) was used for the brain tasks. The participants ' RRIs were measured at rest (denoted as Rest 1) for 7 minutes, while standing (denoted as Standing) for 7 minutes, and during mental arithmetic (denoted as Brain Task 1) for 7 minutes. A 5-minute break was provided between each state(Fig. 5.1(a)). The participants completed 5 sets of these experiments.

In Experiment 2, Sudoku[53] (Fig. 5.1(d)) was used for the brain tasks. The participants ' RRIs were measured at rest (denoted as Rest 2) for 7 minutes and during Sudoku (denoted as Brain Task 2) for 7 minutes. A 5-minute break was provided between each state (Fig. 5.1(a)). The participants completed 5 sets of these experiments.

The reason for adopting Sudoku in Experiment 2 was that the mental arithmetic adopted in Experiment 1 required participants to frequently move their hands to write answers, so the writing load by hand, which is considered a part of physical load, may have affected HRV measurements. Therefore, we chose Sudoku, which

has a low frequency of writing movements, in Experiment 2. If the results differed significantly between Experiment 1 (mental arithmetic) and Experiment 2 (Sudoku), it could be judged that hand movements for writing answers affected the result. In this experiment, mental arithmetic and Sudoku had almost no difference in the tendency of each index; thus, it was considered that there was no influence of writing movement (Table 5.2).

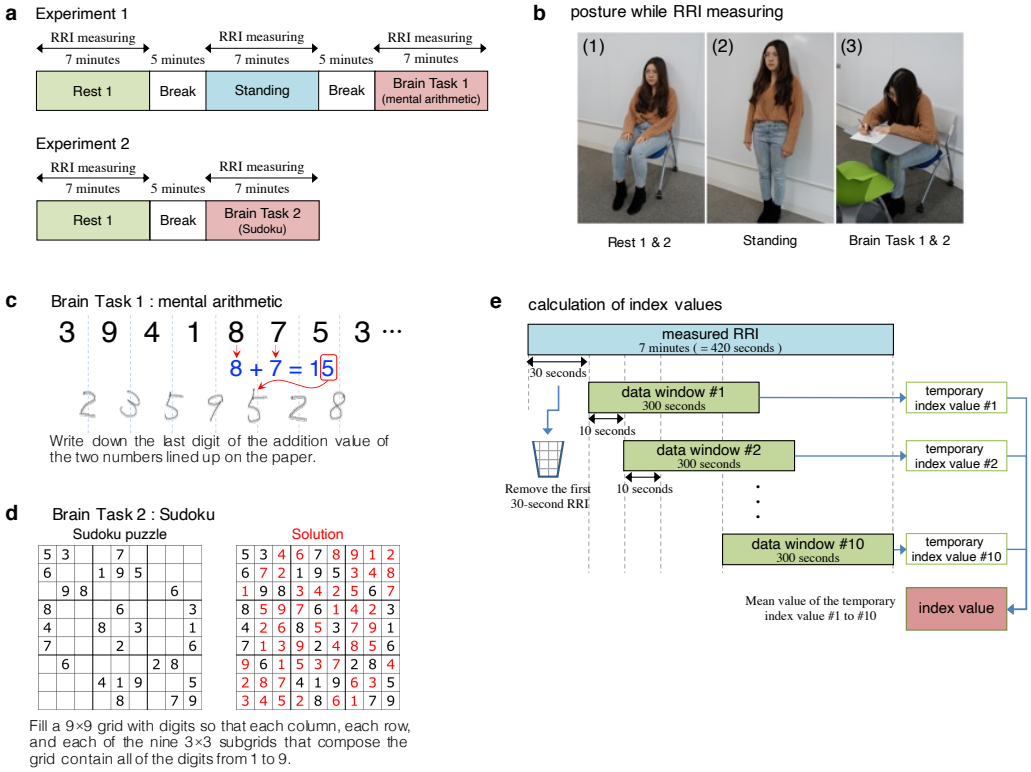

Figure 5.1: Figures to explain the experiment. **(a)** Procedure of measuring RRIs in Experiment 1 and Experiment 2. Participants were given a 5-minute break between 7-minute RRI measurements. **(b-1)** Posture when measuring RRIs in the Rest state. **(b-2)** Posture when measuring RRIs in the Standing state. **(b-3)** Posture when measuring RRIs in the Brain Task state. **(c)** Image of performing mental arithmetic adopted in the Brain Task 1. **(d)** Image of performing Sudoku adopted in the Brain Task 2. **(e)** Procedure of calculation of each index value excluding fractal dimension and SD1/SD2. The first 30 seconds of the 420-second measured RRI were removed, and then 10 temporary index values were calculated using a 300-second data window taken out from the remaining 390-second RRI while sliding for 10 seconds. The index value is given as the average of 10 temporary index values.

Index	Meaning	Units	Description
time-domain analysis			
SDNN	PSNS	ms	Standard deviation of all NN intervals.
SDSD	PSNS	ms	Standard deviation of differences between adjacent NN intervals.
RMSSD	PSNS	ms	The square root of the mean of the sum of the squares of differences between adjacent NN intervals.
pNN50	PSNS	-	The number of pairs of adjacent NN intervals greater than 50 ms / the total number of NN intervals.
$CV_{R\text{-}R}$	PSNS	%	Standard deviation of NN intervals / Mean of NN intervals * 100.
frequency-domain analysis			
LF	SNS	ms^2	Power in low frequency range (0.04Hz-0.15Hz).
HF	PSNS	ms^2	Power in high frequency range (0.15Hz-0.4Hz).
LF/HF	SNS	-	Ratio LF / HF.
LFnorm	SNS	%	Ratio LF / (LF+HF) * 100.
HFnorm	PSNS	%	Ratio HF / (LF+HF) * 100.
chaotic/complexity analysis			
ApEn	-	-	Irregularity rate in time series data.
SampEn	-	-	Irregularity rate in time series data (Improved method of ApEn).
Fractal Dimension	-	-	Self-similarity in the time series data (Higuchi dimension).
SD1/SD2	-	-	Standard deviation along the minor axis in the Poincaréplot (SD1) / Standard deviation along the minor axis in the Poincaréplot (SD2).
CD	-	-	Degree of chaos calculated directly from time series data.
ICD	-	-	Approximate value of the Lyapunov exponent calculated via CD.

Table 5.1: The indices of RRI analysis in Experiments 1 and 2. Upper 5 indices: The indices included in the time-domain analysis. Middle 5 indices: The indices included in the frequency-domain analysis. Lower 6 indices: The indices included in the chaotic/complexity analysis. SNS in the “Meaning” column means that the index is the one for sympathetic nervous system activity, and PSNS means parasympathetic nervous system activity.

5.2.3 RRI analysis

We comprehensively analyzed the RRI data measured in the experiment by using 16 indices (analytical methods) (Table 5.1) selected from the time-domain analysis, frequency-domain analysis, and chaotic/complexity analysis. Each of 14 index values excluding the fractal dimension and SD1/SD2 was calculated as shown in Fig. 5.1(e). That is, the initial 30 seconds of the RRI data were removed, and then the temporary index value was calculated using a sliding window with a length of 300 seconds and a step size of 10 seconds. At this time, 10 temporary index values were calculated for 420 seconds of data. Finally, the index value was given as the average of 10 temporary index values. The remaining two index values, fractal dimension and SD1/SD2, were calculated using all RRI data except the first 30 seconds (i.e., 390-second RRI data).

Time-domain analysis and frequency-domain analysis

Time-domain and frequency-domain analyses have long been used in the fields of HRV analysis and autonomic nerve function evaluation[3]. Using indices included in their analyses, we could determine the activity state of the sympathetic nervous system and/or parasympathetic nervous system. Time-domain analysis evaluates the statistical properties of RRIs. Five indices of SDNN, SDSD, RMSSD, pNN50, and CVR-R that belong to time-domain analysis represent the indices to measure parasympathetic nervous system activation. Frequency-domain analysis assesses the magnitude of power in a particular frequency domain of RRIs. Indices of LF, LF/HF, and LFnorm represent the indices to measure sympathetic nervous system activation, and indices of HF and HFnorm represent the indices to measure parasympathetic nervous system activation.

Chaotic/complexity analysis

HRV analysis is an analysis of ”fluctuations”, but conventional analysis captures only some of the characteristics of RRI fluctuations. Careful observation of the Poincaré plot of RRI (Fig. 5.4) reveals that the possible range of values for the next RRI is narrower as the previous RRI is farther from the mean value and wider as it is closer to the mean value. However, such irregularities and complexity of fluctuations cannot be measured by conventional analysis, as described below.

In the time-domain analysis of the conventional analysis[3], indices that measure the statistical characteristics of the fluctuation of RRI based on the variance or the standard deviation are defined, but it is not quantified how the value of RRI changes step by step. On the other hand, frequency-domain analysis measures the power of periodic components of fluctuations. Aperiodic effects are interpreted as noise. In the case of white noise, a small amount of power appears over the

entire frequency range. In the case of 1/f fluctuation, the power that is inversely proportional to the frequency f appears. However, in the frequency-domain analysis of the conventional analysis[3], there are no indices showing white noise or 1/f fluctuation.

The chaos degree that belongs to the chaotic/complexity analysis described later captures the characteristics of the fluctuations that appear in the Poincaré plot of RRI as "the uncertainty of the possible values of RRI". In Fig. 4.1, it is shown that the indices of CD, ICD, ApEn, SampEn belonging to the chaotic/complexity analysis described later are independent of the indices of SDNN, SDSD, RMSSD belonging to the time-domain analysis of the conventional analysis.

Chaotic/complexity analysis has recently come to be used in the field of HRV analysis and is also the focus of this article. In this article, we defined chaotic/complexity analysis based on the following 6 indices: approximate entropy (ApEn), sample entropy (SampEn), SD1/SD2, fractal dimension, chaos degree (CD), and improved chaos degree (ICD). Details of each index are provided later. The correspondence between chaos in HRV and physiology has not been clearly explained, but some researchers suggest a relation to mental stress. We expected that chaos in HRV would be associated with higher-order brain function in our experiments. In the field of mathematical science, the phenomenon that a simple system (a system with a small degree of freedom) causes random-like behavior is called chaos. Today, chaos is known to exist in various mathematical models, such as natural phenomena, social phenomena, and economic systems. Therefore, the chaos phenomenon may be observed in vital data such as ECG and EEG scans. One of the main conditions for a system to cause chaos is that the system has a property called "sensitivity to initial conditions", which is quantified using an index called the Lyapunov exponent. However, it is necessary to know the dynamical system (i.e., the difference equation of the system) to calculate the Lyapunov exponent. On the other hand, recently, it has become clear that chaos is closely related to conditional entropy, which is defined in the field of information theory. In addition, a method for estimating the Lyapunov exponent via conditional entropy has been developed, which can be calculated using only given data and does not require information about the dynamical system. Details are shown in subsection of CD and ICD. Five of the six indices included in the chaotic/complexity analysis (ApEn, SampEn, SD1/SD2, CD, ICD) behave similarly to the Lyapunov exponent (Fig. 5.2).

Index	Meaning	(1) Rest 1 and Rest 2	(2) Brain Task 1 and Brain Task 2
time-domain analysis			
SDNN	PSNS	0.703	0.148
SDSD	PSNS	0.49	0.454
RMSSD	PSNS	0.488	0.454
pNN50	PSNS	0.727	0.263
$CV_{R\text{-}R}$	PSNS	0.341	0.0271
frequency-domain analysis			
LF	SNS	0.892	0.00852
HF	PSNS	0.521	0.0551
LF/HF	SNS	0.143	0.247
LFnorm	SNS	0.136	0.247
HFnorm	PSNS	0.137	0.248
chaotic/complexity analysis			
ApEn	-	0.568	0.358
SampEn	-	0.276	0.0356
Fractal Dimension	-	0.225	0.0271
SD1/SD2	-	0.474	0.263
CD	-	0.524	0.0722
ICD	-	0.698	0.0407

Table 5.2: P-values as the result of the statistical significance test between Rest 1 and Rest 2 states and between Brain Task 1 and Brain Task 2 states. (1) Comparison between Rest 1 and Rest 2 states. (2) Comparison between Brain Task 1 (mental arithmetic) and Brain Task 2 (Sudoku) states. Upper 5 indices: The indices included in the time-domain analysis. Middle 5 indices: The indices included in the frequency-domain analysis. Lower 6 indices: The indices included in the chaotic/complexity analysis. SNS in the "Meaning" column means that the index is the one for sympathetic nervous system activity, and PSNS means parasympathetic nervous system activity. We investigated whether there was a significant difference between the Rest states of Experiment 1 and Experiment 2 and whether there was a significant difference between the Brain Task states of Experiment 1 and Experiment 2. Considering the p-values listed in the table comprehensively, no difference was considered to be between Rest 1 and Rest 2 states or between Brain Task 1 and Brain Task 2 states. Since there was no correspondence between the data in Experiment 1 and Experiment 2, the Mann-Whitney U test was used for the statistical significance test.

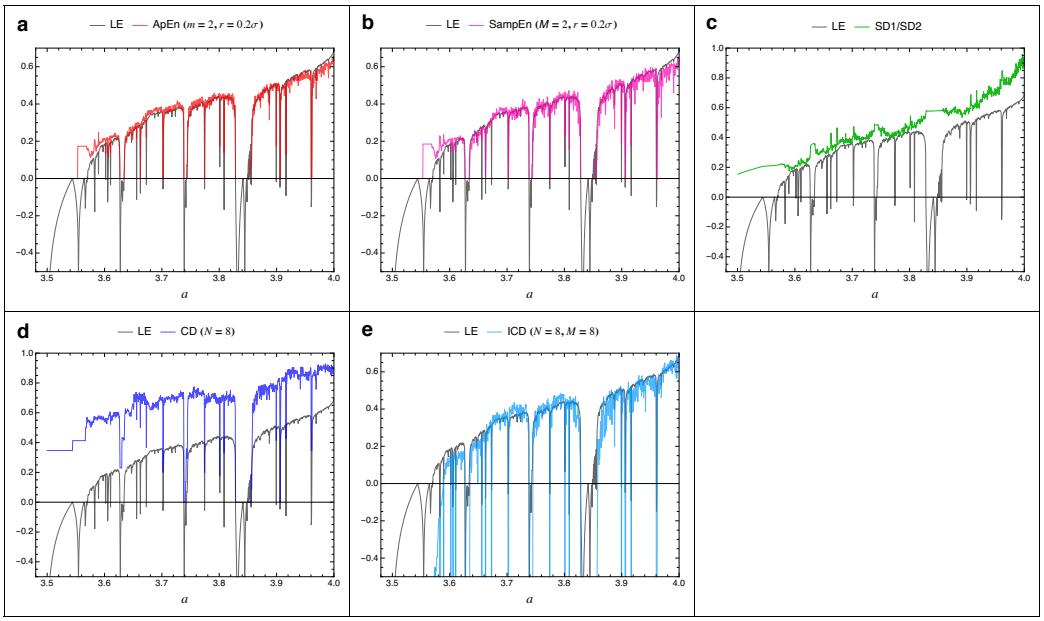

Figure 5.2: Comparison of Lyapunov exponent (LE) and chaos indices (ApEn, SampEn, SD1/SD2, CD, and ICD) of Logistic map. **(a)** ApEn and LE. **(b)** SampEn and LE. **(c)** SD1/SD2 and LE. **(d)** CD and LE. **(e)** ICD and LE. In each figure from (a) to (e), the black solid line shows LE of the logistic map, $x_{n+1} = ax_n(1 - x_n)$, at its control parameter a. Intervals where LE is positive are chaos region, and the larger LE is, the stronger chaos. In contrast, intervals where LE is negative are nonchaos region (i.e., the periodic region). ApEn and SampEn give good approximations of LE, but the computational complexity is $O(n^2)$ for data size n. CD has a numerical difference from LE, but it behaves almost the same as LE. ICD has a value closer to LE. The computational complexity of CD and ICD is $O(n)$ for data size n. Therefore, it is much more advantageous to use CD or ICD.

ApEn[54, 55] and SampEn[28, 29] When time series data contain repeating patterns, values are easier to predict than when such patterns do not exist. ApEn measures the frequency of patterns contained in time series data and quantifies these patterns by the amount of information provided. A large ApEn value means that the pattern is repeated infrequently and the data are complex. ApEn was developed as an improvement on Kolmogorov-Sinai (KS) entropy in order to properly measure the regularity rate in time series data and is used in medical field measurements, such as heart rate, and in financial field measurements. SampEn is a measure of complexity similar to ApEn and is a modified version of ApEn. Macroscopically (if we ignore minor differences), SampEn shows almost the same behavior as ApEn.

Fractal Dimension (Higuchi Dimension)[56, 57] The fractal dimension is a statistical method to quantify complexity and is explained as being derived from self-similarity. As a property of the fractal dimension, its value does not always show an integer value, and a large value means that the data are complex. Some practical methods have been proposed. In this article, we used the Higuchi dimension.

SD1/SD2[58, 59] SD1/SD2 is explained using Poincaré plot shown in Fig. 5.4. That is, SD1 is the standard deviation along the minor axis, i.e., the thickness of the ellipse viewed from the direction of $y = x$ (major axis). SD2 is the standard deviation along the major axis, i.e., the thickness of the ellipse viewed from the direction perpendicular to $y = x$ (minor axis). In particular, a large SD2 value means that the heart rate variability (HRV) is large, that is, the uncertainty is large. Therefore, if SD2 is relatively larger than SD1, the indices of complexity are large. In addition, SD1 and SD2 are highly correlated with SDNN and SDSD, respectively, in the time-domain analysis.

CD[15, 16]and ICD (Improved CD)[23, 30] The Lyapunov exponent is commonly used as a measure of chaos. However, it is difficult to calculate Lyapunov exponents if equations of dynamical systems are not given. On the other hand, Entropic CD [15] is proposed as another measure of chaos that can be directly calculated from data. The definition of CD in difference equations is as follows. We assume that the one dimensional difference equation is determined by a map $f : I \to I(\equiv [a, b] \in \mathbb{R}^1,\ a, b \in \mathbb{R})$, i.e.,$M + 1$ length observed data $\{x_0, x_1, x_2, \cdots, x_M\}(\equiv \{x_n\}_{n=0}^{M})$ is given by $x_{n+1} = f(x_n)$ $(n = 0, 1, 2, \cdots, M-1)$ for $x_0 \in I$. $A = \{A_i\}$ be a finite partition of I such that

$$I = \bigcup_{i=1}^{N} A_i, \quad A_i \cap A_j = \phi\ (i \neq j). \tag{5.2.1}$$

The probability distribution $p(i)$ and the joint probability distribution $p(i, j)$ are given as

$$p(i) = \frac{\#\{x_n \in A_i \mid n = 0, 1, \cdots, M-1\}}{M}, \tag{5.2.2}$$

$$p(i, j) = \frac{\#\{x_n \in A_i,\ x_{n+1} \in A_j \mid n = 0, 1, \cdots, M-1\}}{M}. \tag{5.2.3}$$

Then, CD for $\{x_n\}_{n=0}^{M}$ is defined by

$$\mathrm{CD} = \sum_{i=1}^{N}\sum_{j=1}^{N} p(i, j) \log \frac{p(i)}{p(i, j)} = -\sum_{i=1}^{N} p(i) \sum_{j=1}^{N} p(j|i) \log p(j|i). \tag{5.2.4}$$

where the conditional probability $p(j|i)$ is defined as $p(j|i) = p(i,j)/p(i)$.

There is a difference between the CD and the Lyapunov exponent due to the finite partition. The difference can be interpreted as the amount of information about how the output data $f(A_i)$ are distributed in each A_j. The ICD, which is obtained by subtracting the amount of information from the CD, is defined as follows. In addition to the definition of CD above, $q(i,j)$ is defined as the ratio of $f(A_i)$, which is the area where A_i is mapped by f, to A_j, that is,

$$q(i,j) = \frac{\|f(A_i) \cap A_j\|}{\|A_j\|}. \tag{5.2.5}$$

ICD [23, 30] is defined by subtracting the average amount of information $-\log q(i,j)$ from CD as

$$\mathrm{ICD} = -\sum_{i=1}^{N} p(i) \sum_{j=1}^{N} p(j|i) \log\{p(j|i) - q(i,j)\}. \tag{5.2.6}$$

Computation of $q(i,j)$ using observed data $\{x_n\}_{n=0}^{M}$ is as follows. The component A_j is divided into Q equipartition $B_{j,l}$ such that

$$A_j = \bigcup_{l=1}^{Q} B_{j,l}, \quad B_{j,l} \cap B_{j,l'} = \phi \ (l \neq l'). \tag{5.2.7}$$

Then,

$$q(i,j) = \frac{\#\{\ \#\{x_n \in A_i,\ x_{n+1} \in B_{j,l} \mid n = 0, 1, 2, \cdots, M-1\} > 0 \mid l = 1, 2, \cdots, Q\}}{Q}. \tag{5.2.8}$$

5.2.4 Statistical significance test

The main purpose of this study was to investigate the difference between Rest and Standing outcomes and the difference between Rest and Brain Task outcomes. We performed a statistical significance test among the following three pairs of groups for each index: (1) Rest 1 and Standing, (2) Rest 1 and Brain Task 1, and (3) Rest 2 and Brain Task 2. Data were evaluated using the Wilcoxon signed-rank test, which does not assume data normality, with a significance level of 1%.

5.3 Results

We conducted two experiments to clarify the difference in phenomena that can be captured by each of the conventional time-domain and frequency-domain

indices and the chaos/complexity indices in HRV (Fig. 5.1(a), Methods section). In this experiment, we measured HRV in physical load due to standing posture, which has been conventionally used for evaluation of autonomic nervous function, and in mental load related to brain activity (cognition, mood, anxiety, stress, etc.) and then comprehensively analyzed the RRI using 16 indices selected from time-domain analysis, frequency-domain analysis, and chaotic/complexity analysis (Table 5.1, Methods section).

In Experiment 1, the RRI was measured in three states: Rest 1, Standing, and Brain Task 1. In Experiment 2, the RRI was measured in two states: Rest 2 and Brain Task 2. There was no difference between Rest 1 and Rest 2, but mental arithmetic was used for Brain Task 1, and Sudoku was used for Brain Task 2 (Fig. 5.1(c), Fig. 5.1(d), Methods section). The mean and standard deviation of 16 indices in each state are shown in Table 5.3, and its box-and-whisker plot is shown in Fig. 5.3. The main focus of this study was to investigate the difference between outcomes in the Rest and Standing states and the difference between Rest and Brain Task outcomes. Table 5.4 shows the results of the statistical significance test (p-value) between the following pairs of states; (1) Rest 1 and Standing, (2) Rest 1 and Brain Task 1, and (3) Rest 2 and Brain Task 2.

From Table 5.4, the following tendency can be seen overall. From the viewpoint of conventional autonomic nervous system analysis (time-domain analysis and frequency-domain analysis), indices of parasympathetic nervous system activity significantly decreased and indices of sympathetic nervous system activity significantly increased from the Rest state to the Standing state. In contrast, indices of parasympathetic nervous system activity slightly decreased from the Rest state to the Brain Task states. On the other hand, from the viewpoint of chaotic/complexity analysis, all 6 indices significantly decreased from the Rest state to the Standing state and significantly increased from the Rest state to the Brain Task states. The characteristics of HRV, which are supposed to be related to a marked increase in indices of chaotic/complexity analysis during Brain Task performance, can also be visually confirmed by a Poincaré plot (Fig. 5.4).

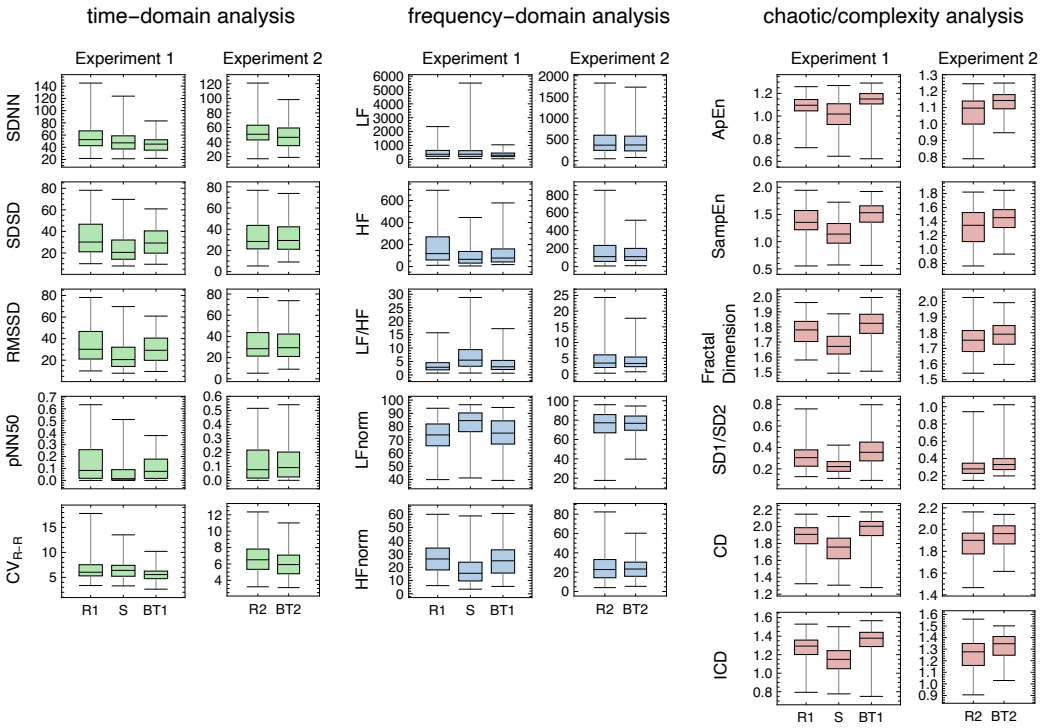

Figure 5.3: Box-and-whisker plot of the results of Experiment 1 and Experiment 2. Left side: The indices included in the time-domain analysis. Center: The indices included in the frequency-domain analysis. Right side: The indices included in the chaotic/complexity analysis. The number of data points (sample size) was 90 (= 18[participants] $\times$ 5[times]). R1 and R2 mean the Rest 1 and Rest 2 states, respectively. BT1 and BT2 mean the Brain Task 1 and Brain Task 2 states, respectively. S means the Standing state.

	Experiment 1						Experiment 2			
	Rest 1		Standing		Brain Task 1		Rest 2		Brain Task 2	
	μ	σ	μ	σ	μ	σ	μ	σ	μ	σ
time-domain analysis										
SDNN	55.89	19.98	50.72	19.51	44.42	11.31	54.63	19.93	48.96	16.93
SDSD	34.06	16.03	23.96	12.80	30.23	11.99	32.26	15.29	32.04	13.66
RMSSD	34.06	16.03	23.96	12.80	30.23	11.99	32.26	15.29	32.04	13.66
pNN50	0.14	0.14	0.06	0.09	0.10	0.10	0.13	0.14	0.13	0.12
$CV_{R\text{-}R}$	6.56	2.19	6.68	2.00	5.51	1.28	6.70	1.95	6.06	1.60
frequency-domain analysis										
LF	508.73	451.75	527.73	667.81	328.72	195.68	467.95	335.12	447.02	309.18
HF	197.17	184.10	103.91	101.54	112.52	96.33	178.21	173.41	134.63	96.60
LF/HF	3.59	2.53	7.14	5.38	4.24	3.38	4.57	3.79	4.30	2.92
LFnorm	72.85	11.50	82.49	10.21	74.83	11.25	74.20	15.60	76.50	10.00
HFnorm	27.15	11.50	17.51	10.21	25.17	11.25	25.80	15.60	23.50	10.00
chaotic/complexity analysis										
ApEn	1.08	0.11	1.01	0.13	1.14	0.10	1.07	0.11	1.13	0.07
SampEn	1.36	0.27	1.14	0.26	1.48	0.24	1.32	0.27	1.44	0.20
Fractal Dimension	1.77	0.09	1.67	0.09	1.81	0.09	1.75	0.10	1.79	0.08
SD1/SD2	0.31	0.12	0.23	0.07	0.38	0.15	0.31	0.13	0.36	0.16
CD	1.88	0.16	1.75	0.18	1.96	0.15	1.87	0.16	1.94	0.11
ICD	1.27	0.14	1.16	0.16	1.35	0.14	1.26	0.14	1.33	0.10

Table 5.3: Index values as experimental results : Mean μ and standard deviation σ of index values in each state in Experiment 1 and 2. Upper 5 indices: The indices included in the time-domain analysis. Middle 5 indices: The indices included in the frequency-domain analysis. Lower 6 indices: The indices included in the chaotic/complexity analysis. The number of data points (sample size) was 90 (= 18[participants] $\times$ 5[times]).

Index	Meaning	(1) Rest 1 → Standing		(2) Rest 1 → Brain Task 1		(3) Rest 2 → Brain Task 2	
		p-value	Direction of change	p-value	Direction of change	p-value	Direction of change
time-domain analysis							
SDNN	PSNS	0.00433	↓	9.59E-9	↓	0.00043	↓
SDSD	PSNS	6.93E-15	↓	0.00214	↓	0.44	↓
RMSSD	PSNS	6.93E-15	↓	0.00214	↓	0.44	↓
pNN50	PSNS	7.9E-14	↓	0.00298	↓	0.486	↓
$CV_{R\text{-}R}$	PSNS	0.391	↑	2.99E-6	↓	0.00238	↓
frequency-domain analysis							
LF	SNS	0.831	↑	0.00059	↓	0.541	↓
HF	PSNS	3.77E-14	↓	4.61E-7	↓	0.0135	↓
LF/HF	SNS	7.47E-12	↑	0.095	↑	0.917	↓
LFnorm	SNS	2.E-10	↑	0.0822	↑	0.116	↑
HFnorm	PSNS	2.E-10	↓	0.0822	↓	0.116	↓
chaotic/complexity analysis							
ApEn	-	3.66E-7	↓	1.79E-6	↑	1.8E-7	↑
SampEn	-	5.15E-11	↓	0.00015	↑	2.E-5	↑
Fractal Dimension	-	7.15E-15	↓	2.18E-6	↑	4.91E-5	↑
SD1/SD2	-	9.09E-12	↓	2.52E-5	↑	1.39E-5	↑
CD	-	2.E-10	↓	1.36E-5	↑	5.05E-6	↑
ICD	-	6.56E-10	↓	1.79E-6	↑	8.74E-6	↑

Table 5.4: P-values as a result of the statistical significance test of the difference between two groups, and the direction of change (increase or decrease) of the mean value of the index when compared to that at rest state. (1) Comparison between the Rest 1 and the Standing states. (2) Comparison between the Rest 1 and the Brain Task 1 (mental arithmetic) states. (3) Comparison between the Rest 2 and the Brain Task 2 (Sudoku) states. Upper 5 indices: The indices included in the time-domain analysis. Middle 5 indices: The indices included in the frequency-domain analysis. Lower 6 indices: The indices included in the chaotic/complexity analysis. The red or blue background colors indicate that the mean value of the index increased or decreased significantly compared to that at rest. In addition, if the p-value < 0.0001 (especially significance), then the background was painted dark red or dark blue; if $0.0001 \leq$ p-value < 0.01 (significance), then the background was painted light red or light blue. The upward or downward arrow in the "Direction of change" column means that the average index value increased or decreased compared to that in the rest state. SNS in the "Meaning" column means that the index is the one for sympathetic nervous system activity, and PSNS means parasympathetic nervous system activity. The number of data points (sample size) was 90 (= 18[participants] $\times$ 5[times]).

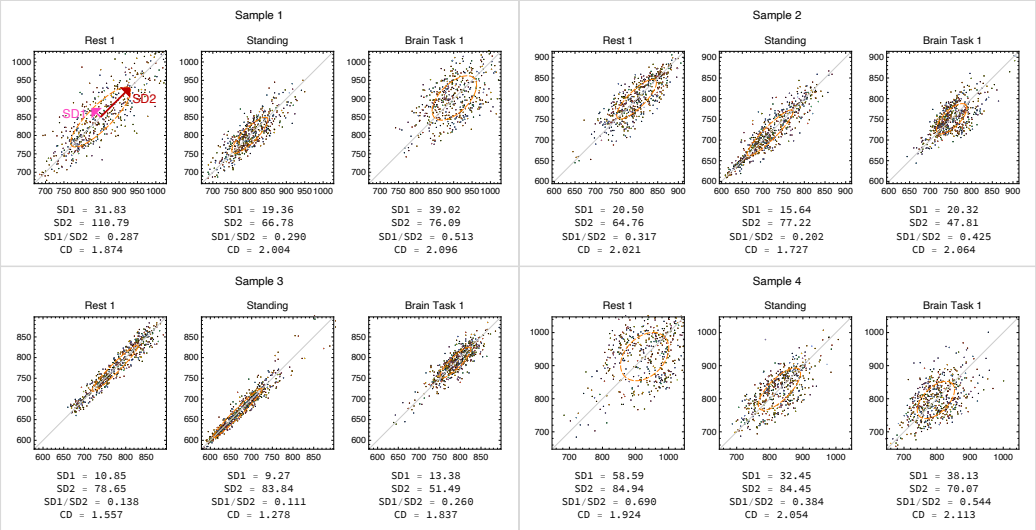

Figure 5.4: Typical examples of RRI Poincaré plots in the Rest 1, Standing, and Brain Task 1 state. The Poincaré plot is a return map that plots points at the positions (x-axis, y-axis) = $(u_1, u_2), (u_2, u_3), (u_3, u_4), \cdots$ where $\{u_1, u_2, u_3, u_4 \ldots\}$ are time series RRI data. Let us look at the ellipse with orange dotted line. SD1 is the standard deviation along the minor axis. SD2 is the standard deviation along the major axis. An increase in the thickness of the Poincaré plot in the minor axis direction, that is, an increase in SD1/SD2 means that the change from the current RRI value u_i to the next value u_{i+1} becomes more widespread and leads to an uncertainty increase in the future. As a result, the chaos degree (CD), which is defined by conditional entropy, also increases. The elliptical shape of the Poincaré plot becomes more elongated in the Standing state than in the Rest state and becomes closer to a perfect circle in the Brain Task state than in the Rest state.

5.4 Discussion

The result that showed a significant superiority of sympathetic nervous system activity in the Standing state was consistent with previous studies using conventional autonomic nervous system function evaluation[3, 60, 61]. In addition, we could provide a plausible reason that the result showed a slight superiority of sympathetic nervous system activity in the Brain Task states by using the NVI model[41, 42] and large-scale brain networks[47, 62, 63, 48, 49](Fig. 4.2).

In the Standing state, all the chaotic/complexity indices were significantly decreased. This result is equivalent to the result reported in a previous study[5] that the conditional entropy of RRI is significantly decreased by a head-up tilt.

Reference[5] explains that a decrease in conditional entropy of RRI is consistent with an increase in Mayer wave (blood pressure related) components and a decrease in respiratory components, which are associated with a decrease in parasympathetic activity and/or an increase in sympathetic activity[39, 60]. Therefore, one of the main periodic components of the RRI is considered to become dominant, and the fluctuation of the RRI is simplified. In this experiment, the increase in the Mayer wave (blood pressure related) component and the decrease in the respiration related component were reflected in the increase in the frequency-domain index LF/HF, the increase in the LFnorm, and the decrease in the HFnorm; thus, it is thought that the same interpretation from previous studies is relevant here as well.

In the Brain Task states, all chaotic/complexity indices were significantly increased. Furthermore, the change in the periodic components (LF/HF, LFnorm, HFnorm) described above associated with sympathetic nervous system activity or parasympathetic nervous system activity was not observed; thus, it is assumed that other factors were involved in the rise in chaotic/complexity indices. In other words, the effect of brain activity during mental arithmetic/Sudoku on HRV could be clearly read from indices based on the viewpoint of chaos/complexity.

From the above, the conventional time-domain and frequency-domain analysis mainly captures the effects of physical load (autonomic nervous regulation by baroreceptor reflex derived from blood pressure fluctuation and respiratory fluctuation), and in contrast, only chaotic/complexity analysis can significantly capture the effects of mental load (higher-order brain functions).

Suggestion (how to distinguish the brain task states) In this experiment, chaotic/complexity indices increased for mental workloads and decreased for physical load. Thus, it may be determined which mental workload or physical load is imposed (if only one of them is imposed) as follows. Let CCI_1 be the chaotic/complexity index (CCI: ApEn, SampEn, fractal dimension, SD1/SD2, CD, and ICD) value in one reference state 1 (such as the Rest states in this experiment) and CCI_2 be the CCI value in another state 2. The ratio γ is defined as

$$\gamma = \frac{CCI_2}{CCI_1}. \tag{5.4.1}$$

Let us call this relation the chaos indicator ratio (CIR). Suppose state 1 is a resting state; if $\gamma > 1$, then state 2 is determined to be a state in which mental workload is imposed; if $\gamma < 1$, then state 2 is determined to be a state in which physical load is imposed. Fig. 5.5 shows the histogram of the CIR γ calculated from these experimental data. The CIR γ of the Standing to Rest states and the ratio of the mental workload when performing mental arithmetic or Sudoku to that in the Rest

states are distributed separately in each region of $\gamma < 1$ and $\gamma > 1$. Therefore, it is possible to universally determine whether mental workload or physical load is imposed by whether the value of CIR that we defined is larger or smaller than 1. Note that it is possible to determine the state universally by CIR, regardless of which chaos index is used. More generally, both physical and mental loads may be added. However, it should be kept in mind that too much difficulty can lead to increased stress and decreased ECN activity[50].

It has been reported that the DMN is slightly deactivated in less difficult brain tasks and familiar/proficient tasks and that ECN activation is large in difficult and unfamiliar tasks[47, 62]. Based on the above, it is inferred that the simpler the problem is, the lower the chaos of the RRI and that the more difficult the problem is, the higher the chaos of the RRI. Therefore, there is a possibility that the activity state of the brain can be quantified (such as the degree of deactivation of the DMN, the degree of activation of the ECN and SN, and the degree of concentration on work) using chaos indices.

In the analysis of biological data, it is a major issue that there are individual differences in index values; if they are extremely different depending on the individual, it is difficult to set thresholds for each individual or to make comparisons between individuals. According to Fig. 5.5, it can be seen that the CIR values exhibit few individual differences. Therefore, CIR has a certain universal indicator characteristic in that it is not easily affected by individual differences.

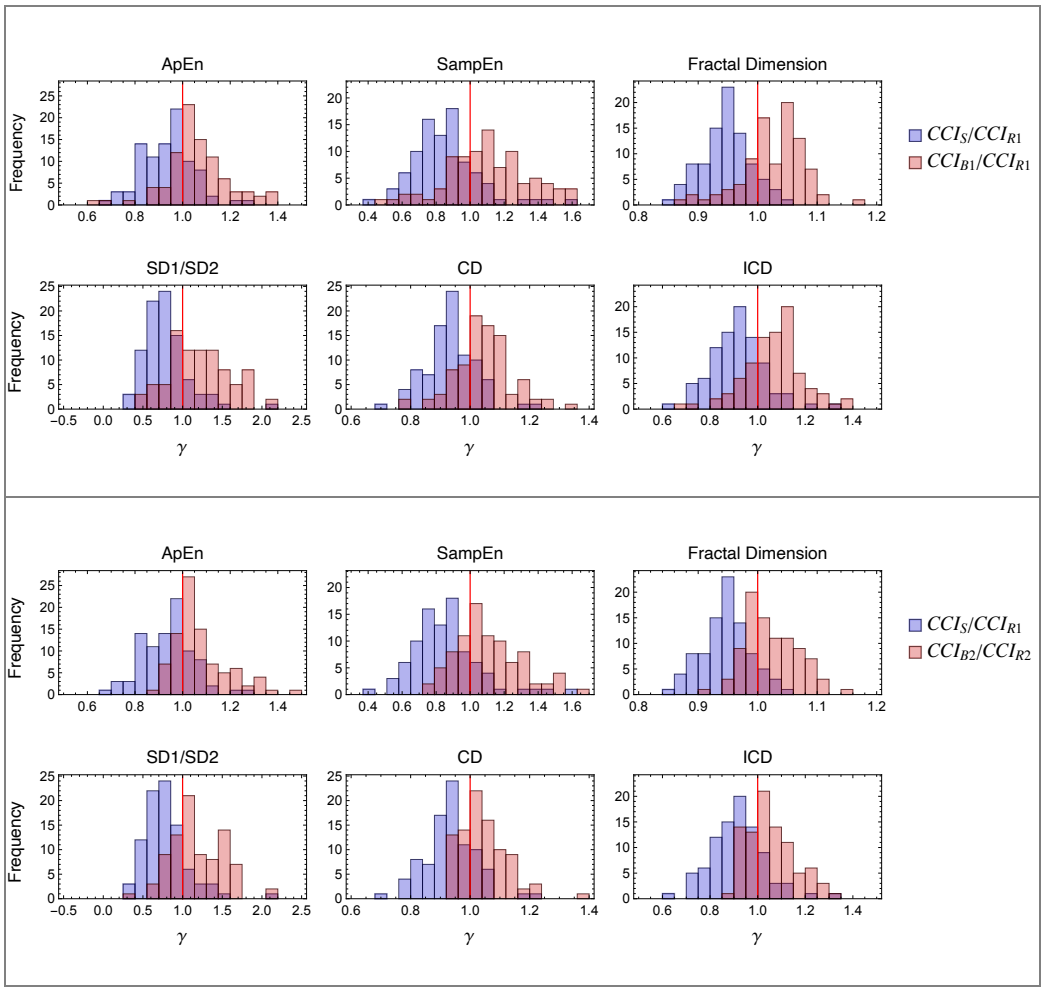

Figure 5.5: Histogram of the chaos indicator ratio (CIR) using 6 indices included in the chaotic/complexity analysis. Upper: CIR of Rest to Standing states (blue) and Rest to Brain Task 1 states (red). Lower: CIR of Rest to Standing states (blue) and Rest to Brain Task 2 states (red). CCI means any of the six indices included in the chaotic/complexity analysis.

5.5 Conclusion

In this experiment, a characteristic tendency was found that the indices of chaos/complexity decreased with physical load and increased with mental workload based on comprehensive RRI analysis using multiple analytical methods. That is, the chaos/complexity indices remarkably capture the characteristics of HRV in mental load, which has not been captured by conventional time-domain

and frequency-domain indices. Focusing on why brain activity in mental arithmetic and Sudoku leads to increased chaos in the heartbeat, we proposed a model that explains interactions between the state of the brain network and the chaotic nature of HRV consistently with previous studies on the neurovisceral integration model and large brain networks. In addition, from an application perspective, we defined the CIR, which can discriminate between the states of mental workload and physical load using chaotic/complexity indices.

This study has revealed that the chaos/complexity indices of HRV, which could not be seen due to the limitations of conventional analytical methods, is extremely significant for understanding the interaction mechanism of important organs such as the human brain and heart.

Importantly, RRI analysis is much easier and less expensive than electroencephalography (EEG) and fMRI in that RRI can be measured with a small heart rate sensor. Therefore, estimating the state of the brain from heart data has great advantages both in terms of technical feasibility and user convenience. It is expected that this research will lead to the development of technology for estimating fatigue, drowsiness, stress, etc. in real time.

Furthermore, the fact that chaos/complexity analysis of RRI has yielded new insights from this basic experiment suggests that it is useful to consider ECG data, which contain more information than RRI, in terms of chaos/complexity. In other words, chaos/complexity analysis is likely to contribute to approaches to unsolved problems such as detection of signs of sudden cardiac death (SCD) and epileptic seizures, in the sense that brain states can be estimated from the chaotic nature of heartbeats, and is expected to be applied to the medical field in the future.

Chapter 6

Conclusion

Let us summarize this thesis.

In Chapter 2, we investigated the properties of chaos degree using asymmetric tent maps, and showed that the difference between chaos degree and Lyapunov exponent is due to the effect of partitioning. Furthermore, we gave an information-theoretic interpretation of the amount of the difference. The limit of the infinite number of divisions of the chaos degree was derived analytically also using asymmetric tent maps. As a result, it was found that the limit values of chaos degree of asymmetric tent maps differ significantly depending on whether the parameter is a rational or irrational number.

In Chapter 3, we defined improved chaos degree as chaos degree from which the amount of information that is the difference between chaos degree and Lyapunov exponent is removed. Furthermore, we proved that improved chaos degree is consistent with discretized Lyapunov exponent. In addition, we confirmed that the computational complexity of improved chaos degree is sufficiently small compared to SampEn. Therefore, improved chaos degree is suitable for real-time analysis.

In Chapter 4, we summarized previous studies on the neuroviceral integration model that explains the relationship between higher brain functions and heart rate control, and previous studies on large-scale brain networks, and added our own discussion, and hypothesized that the chaos appearing in heart rate variability is due to higher brain activity.

In Chapter 5, we conducted experiments to analyze heart rate variability data during brain activities (mental arithmetic and Sudoku) to verify our hypothesis. As a result, the values of the chaos indices increased markedly during brain activity. This was a feature that was not found in any existing analytical index. This result confirms our hypothesis. Furthermore, we found that the change in the chaos indices during brain activity was in the opposite direction compared to that during physical load. This suggests that the chaos index ratio may be used for state discrimination.

The first significance of this study is that it proposed a improved chaos degree with a clear correspondence to Lyapunov exponent as a measure of the chaotic nature of heart rate variability (not only heart rate variability, but also other general data). The second point is that the hypothesis that brain network activity is the cause of the chaos in heart rate variability as an answer to the previously unanswered question of "what does chaos in heart rate variability mean and why does it occur?", and the characteristic experimental results that support the hypothesis were obtained.

In the future, improved chaos degree proposed in this study may become a standard index for chaos analysis of heart rate variability. In other words, chaos analysis using this improved chaos degree can be an effective means to investigate the state of the human body from heart rate variability data that can be measured from the body surface. Several previous studies have suggested that nonlinear analysis of heart rate variability may be applied to the medical field, and analysis using improved chaos degree has the same potential. In particular, if the relationship between the heart and the brain hypothesized in this study is further verified, it is expected to be applied to the detection of signs of epileptic seizures.

Another advantage of improved chaos degree is its low computational complexity. This means that it is suitable for real-time estimation. Furthermore, based on the hypothesis of the relationship between brain activity and heartbeat presented in this study, if the brain state during fatigue or drowsiness can be estimated from heart rate variability data, it can be applied to a system that estimates the driver's state during driving in real time and prevents fatal accidents.

This study has demonstrated a valid method for measuring chaos in heart rate variability and the importance of measuring chaos in heart rate variability. We hope that this study will lead to more information from heart rate variability that has not been available so far, and accelerate approaches to unsolved problems in the medical field.

Acknowledgement

The author, Tomoyuki Mao, would like to express my deepest gratitude to Professor Ken Umeno for finding the significance of this research and accepting me as a working student into the Graduate School, and for his guidance and valuable advice in making substantial progress in this research.

I would like to thank Professor Yoshito Ohta and Associate Professor Satoshi Tsujimoto for their insightful comments and important suggestions from a professional point of view. Professor Ohta has also supported me as an advisor in aspects other than research.

I am also grateful to Dr. Hidetoshi Okutomi, my mentor in Toshiba Information Systems (Japan) Corporation, for not only developing our research as a co-researcher, but also pointing the way for me to enter a graduate school doctoral program.

I am thankful to Professor Kei Inoue of Sanyo-Onoda City University for fruitful discussions that led to the conception of important ideas for this research.

I sincerely thank Sosuke Ito, former president of Toshiba Information Systems (Japan) Corporation, for his understanding and encouragement of my doctoral studies, and Masahiro Tanaka of Toshiba Digital Engineering Corporation and Hiroshi Yamashita and Kazuyuki Nakaya of Toshiba Information Systems (Japan) Corporation for their appropriate management and generous support so that I could concentrate on my studies. I would also like to express my gratitude and respect to Masanori Murabayashi of Toshiba Digital Engineering Corporation, who developed the idea that led to the start of this research.

I would like to thank the students and staff of the Physical Statistics Laboratory, Department of Applied Mathematics and Physics, Graduate School of Informatics, Kyoto University for their positive influence and inspiration. I also deeply appreciate their support in conducting the experiments. The valuable data obtained from the experiments have greatly advanced this research.

The experiments reported in the body of this thesis were conducted with the approval of the Research Ethics Committee of the Graduate School of Informatics, Kyoto University (the approval number: KUIS-EAR-2019-006).

Appendix A

Experiment to measure and analyze heart rate variability in a driver and a fellow passenger during driving

A.1 Introduction

As discussed in the body of the thesis, chaos analysis of heart rate variability has potential applications in understanding the real-time status of car drivers and preventing accidents.

In this chapter, we report on a preliminary experiment to measure heart rate variability of a driver and a passenger in the front seat of a car during actual driving.

A.2 Methods

One driver and one passenger in the front passenger seat wore a heart rate sensor (Polar H10) to measure RRI data during the ride. Three passengers who did not participate in the measurements rode in the back seat.

The route was a road trip from near Kyoto Station to an accommodation near the Sumoto Interchange on Awaji Island, including an expressway. Measurements were taken on both the outbound and inbound routes, but they were not exactly the same routes because of a visit to a museum facility on the return trip. Measurements were taken not only while the vehicle was in motion, but also continuously while the vehicle was stopped at rest stops such as service areas. No restrictions were placed on the activities of participants at the rest stops.

The RRI data were analyzed using a 5-minute sliding window, and heart rate, SDNN, SDSD, RMSSD, pNN50, LF, HF, HFR (HFnorm), HF/LF, CD (chaos

degree), and ICD (improved chaos degree) were calculated as analysis indices.

A.3 Results

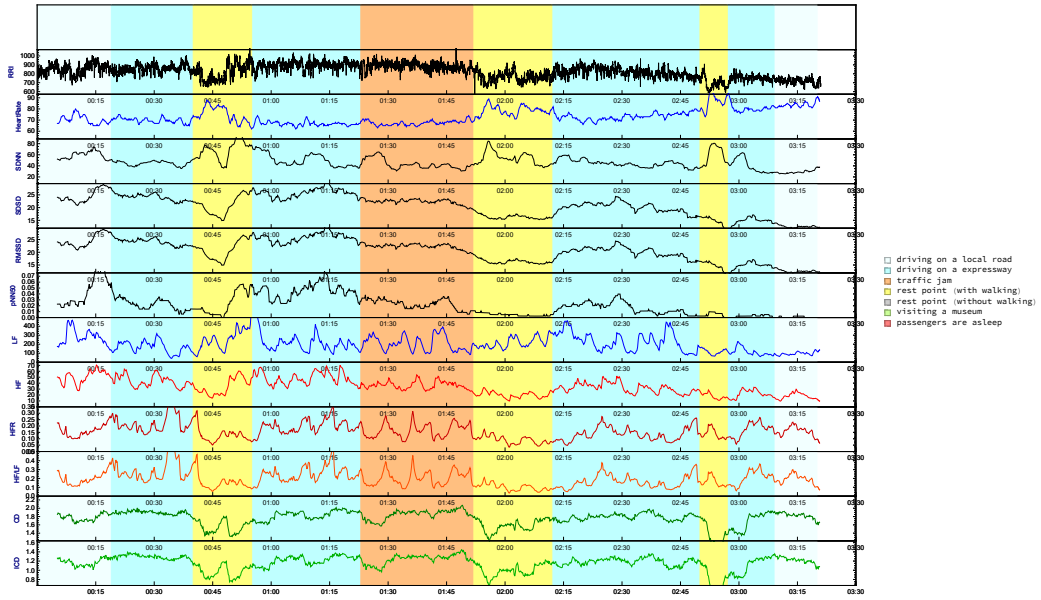

Figure A.1: RRI and heart rate variability analysis indices for the driver on the outbound travel route.

Results are shown in Figs.A.1, A.2, A.3, and A.4. There was a traffic jam between 1:23 and 1:52 on the outbound route. On the return trip, between 0:38 and 2:12, the driver and passenger exited the car and walked to visit the museum facilities. On the return trip, between 5:19 and 5:43, the passenger in the front seat was asleep. At this time, there was a large increase in HF of the passenger in association with the change in respiration with sleep. During the same period, all rear seat passengers were asleep, and the driver also felt drowsy.

A.4 Discussion

The chaos degree and improved chaos degree of heart rate variability decreased when the participants got out of the car and walked while stopped at the rest stop. This is consistent with the fact that the chaos indices significantly decreased during standing in the experiment described in the main text of the thesis.

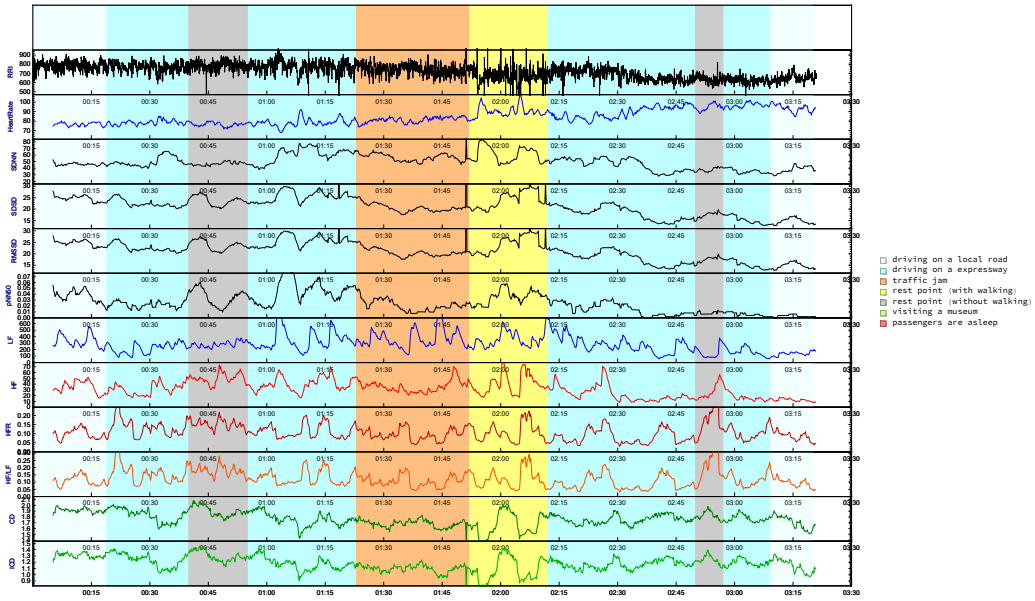

Figure A.2: RRI and heart rate variability analysis indices for the front seat passenger on the outbound travel route.

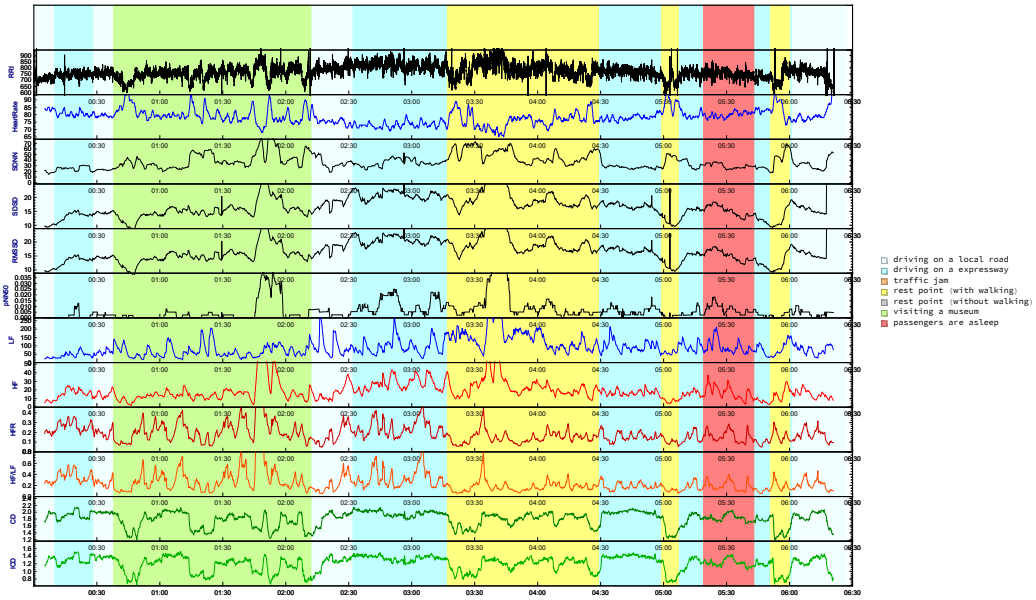

Figure A.3: RRI and heart rate variability analysis indices for the driver on the inbound travel route.

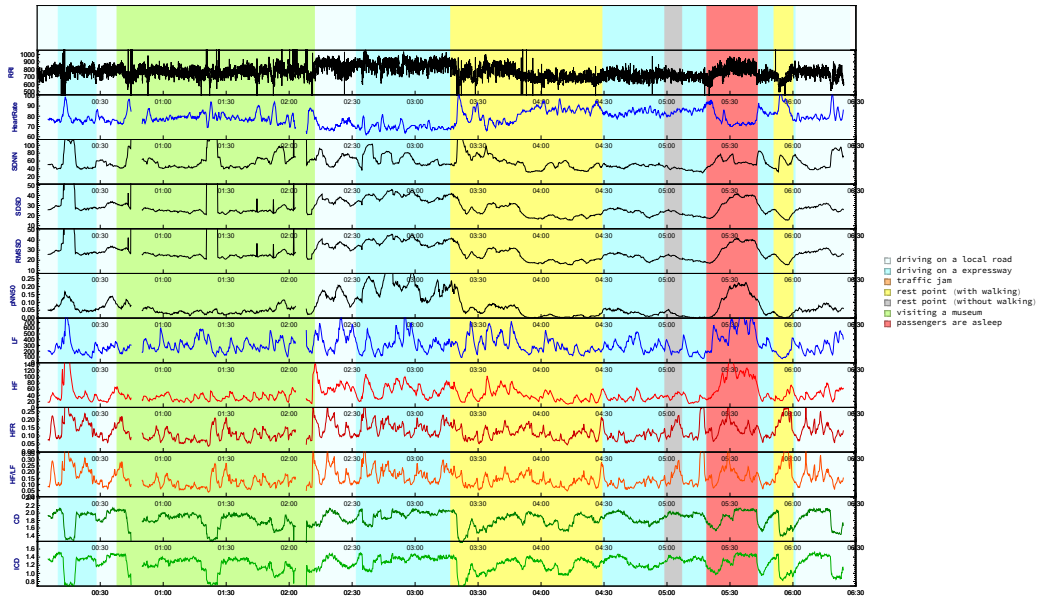

Figure A.4: RRI and heart rate variability analysis indices for the front seat passenger on the inbound travel route.

The chaos degree and improved chaos degree decreased and re-elevated when the passenger in the front seat fell asleep and awoke. Similar declines and rises were also observed when the driver felt sleepy after entering a traffic jam, although the declines were smaller.

The characteristics of these changes in the chaos indices may be related to signs of drowsiness. Based on the hypotheses presented in the body text, it is possible that some change in brain activity during the transition from wakefulness to sleep may have manifested itself in the chaotic nature of heart rate variability.

A.5 Conclusion

Although it is not yet possible to draw definitive conclusions, the results of this experiment indicate that chaos analysis of heart rate variability has great potential to provide important information for real-time estimation of physiological state during driving.

Future work is needed to increase the number of subjects and the number of experiments to determine whether this is a reproducible phenomenon.

Bibliography

[1] M. N. Levy. Autonomic interactions in cardiac controla. Annals of the New York Academy of Sciences, 601(1):209–221, 1990.

[2] J. P. Saul. Beat-to-beat variations of heart rate reflect modulation of cardiac autonomic outflow. Physiology, 5(1):32–37, 1990.

[3] M. Malik, J. T. Bigger, A. J. Camm, R. E. Kleiger, A. Malliani, A. J. Moss, and P. J. Schwartz. Heart rate variability: Standards of measurement, physiological interpretation, and clinical use. European Heart Journal, 17(3):354–381, 1996.

[4] T. A. Denton, G. A. Diamond, R. H. Helfant, S. Khan, and H. Karagueuzian. Fascinating rhythm: A primer on chaos theory and its application to cardiology. American Heart Journal, 120(6, Part 1):1419–1440, 1990.

[5] M. Valente, M. Javorka, Z. Turianikova, B. Czippelova, J. Krohova, G. Nollo, and L. Faes. Cardiovascular and respiratory variability during orthostatic and mental stress: A comparison of entropy estimators. In 2017 39th Annual International Conference of the IEEE Engineering in Medicine and Biology Society (EMBC), pp. 3481–3484, 2017.

[6] E. Blons, L. M. Arsac, P. Gilfriche, H. Mcleod, V. Lespinet-Najib, E. Grivel, and V. Deschodt-Arsac. Alterations in heart-brain interactions under mild stress during a cognitive task are reflected in entropy of heart rate dynamics. Scientific Reports, 9:18190, 2019.

[7] D. A. Dimitriev, E. V. Saperova, and A. D. Dimitriev. State anxiety and nonlinear dynamics of heart rate variability in students. PLOS ONE, 11(1):e0146131, 2016.

[8] H. Young and D. Benton. We should be using nonlinear indices when relating heart-rate dynamics to cognition and mood. Scientific Reports, 5:16619, 2015.

[9] F. Sessa, V. Anna, G. Messina, G. Cibelli, V. Monda, G. Marsala, M. Ruberto, A. Biondi, O. Cascio, G. Bertozzi, D. Pisanelli, F. Maglietta, A. Messina, M. P. Mollica, and M. Salerno. Heart rate variability as predictive factor for sudden cardiac death. Aging, 10(2):166–177, 2018.

[10] K. Majerova, M. Zvarik, I. Ricon-Becker, T. Hanalis-Miller, I. Mikolaskova, V. Bella, B. Mravec, and L. Hunakova. Increased sympathetic modulation in breast cancer survivors determined by measurement of heart rate variability. Scientific Reports, 12(1):1–10, 2022.

[11] F. Takens. Detecting strange attractors in turbulence. In D. Rand and L.-S. Young eds., Dynamical Systems and Turbulence, Warwick 1980, pp. 366–381, Berlin, Heidelberg, 1981. Springer Berlin Heidelberg.

[12] A. Wolf, J. B. Swift, H. L. Swinney, and J. A. Vastano. Determining lyapunov exponents from a time series. Physica D: Nonlinear Phenomena, 16(3):285–317, 1985.

[13] M. T. Rosenstein, J. J. Collins, and C. J. De Luca. A practical method for calculating largest lyapunov exponents from small data sets. Physica D: Nonlinear Phenomena, 65(1):117–134, 1993.

[14] H. Kantz. A robust method to estimate the maximal lyapunov exponent of a time series. Physics Letters A, 185(1):77–87, 1994.

[15] M. Ohya. Complexities and their applications to characterization of chaos. International Journal of Theoretical Physics, 37:495–505, 1998.

[16] T. Mao, H. Okutomi, and K. Umeno. Investigation of the difference between chaos degree and Lyapunov exponent for asymmetric tent maps. JSIAM Letters, 11:61–64, 2019.

[17] T. Mao, H. Okutomi, and K. Umeno. Analysis of the limit values of chaos degree for infinite number of partitions in asymmetric tent maps. JSIAM Letters (Conditional accepted on 2022/11/24).

[18] K. Inoue, M. Ohya, and K. Sato. Application of chaos degree to some dynamical systems. Chaos, Solitons & Fractals, 11(9):1377–1385, 2000.

[19] K. Inoue. Basic properties of entropic chaos degree in classical systems. INFORMATION, 16(12(B)):8589–8596, 2013.

[20] K. Inoue. On evaluation of quasi-periodic orbits by chaos degree (in japanese). Transactions of the Japan Society for Industrial and Applied Mathematics, 25:105–115, 2015.

[21] T. Kamizawa, T. Hara, and M. Ohya. On relations among the entropic chaos degree, the kolmogorov-sinai entropy and the lyapunov exponent. Journal of Mathematical Physics, 55(3):032702, 2014.

[22] H. Okutomi and T. Mao. Mathematical relationship between chaos degree and lyapunov exponent (in japanese). IEICE Tech. Rep., 117(288):5–10, 2017.

[23] T. Mao, H. Okutomi, and K. Umeno. Proposal of improved chaos degree based on interpretation of the difference between chaos degree and lyapunov exponent (in japanese). Transactions of the Japan Society for Industrial and Applied Mathematics, 29:383–394, 2019.

[24] E. M. Stein and R. Shakarchi. Fourier Analysis: An Introduction (Princeton Lectures in Analysis, Volume 1). Princeton University Press, Princeton, New Jersey, 2011.

[25] 池口徹, 山田泰司, 小室元政, 合原一幸 (編). カオス時系列解析の基礎と応用. 産業図書, 2000.

[26] 岡田大樹, 梅野健. 新たな非線形時系列解析の手法－移動最大リアプノフ指数線によるカオス解析－. レーザー研究, 43:359–364, 2015.

[27] 大矢雅則, 原利英. 数理物理と数理情報の基礎. 近代科学社, 2016.

[28] J. S. Richman and J. R. Moorman. Physiological time-series analysis using approximate entropy and sample entropy. American Journal of Physiology-Heart and Circulatory Physiology, 278:H2039–H2049, 2000.

[29] A. Delgado-Bonal and A. Marshak. Approximate entropy and sample entropy: A comprehensive tutorial. Entropy, 21, 2019.

[30] K. Inoue, T. Mao, H. Okutomi, and K. Umeno. An extension of the entropic chaos degree and its positive effect. Japan Journal of Industrial and Applied Mathematics, 38:611–624, 2019.

[31] T. Mao, H. Okutomi, and K. Umeno. Chaotic fluctuations in heart rate variability associated with interaction of large-scale brain networks: experiments and hypotheses. PREPRINT (Version 1) available at Research Square [https://doi.org/10.21203/rs.3.rs-2190064/v1], November 2022.

[32] A. L. Goldberger. Non-linear dynamics for clinicians: chaos theory, fractals, and complexity at the bedside. The Lancet, 347(9011):1312–1314, 1996.

[33] A. L. Goldberger. Fractal variability versus pathologic periodicity: Complexity loss and stereotypy in disease. Perspectives in Biology and Medicine, 40(4):543–561, 1997.

[34] F. Lombardi. Chaos theory, heart rate variability, and arrhythmic mortality. Circulation, 101(1):8–10, 2000.

[35] R. M. May. Simple mathematical models with very complicated dynamics. Nature, 261:459–467, 1976.

[36] E. N. Lorenz. Deterministic nonperiodic flow. Journal of the Atmospheric Sciences, 20:130–141, 1963.

[37] D. C. Michaels, D. R. Chialvo, E. P. Matyas, and J. Jalife. Chaotic activity in a mathematical model of the vagally driven sinoatrial node. Circulation Research, 65:1350–1360, 1989.

[38] I. Hagerman, M. Berglund, M. Lorin, J. Nowak, and C. Sylvén. Chaos-related deterministic regulation of heart rate variability in time- and frequency domains: effects of autonomic blockade and exercise. Cardiovascular Research, 31:410–418, 1996.

[39] J. Taelman, S. Vandeput, I. Gligorijević, A. Spaepen, and S. Van Huffel. Time-frequency heart rate variability characteristics of young adults during physical, mental and combined stress in laboratory environment. In 2011 Annual International Conference of the IEEE Engineering in Medicine and Biology Society, pp. 1973–1976, 2011.

[40] E. E. Benarroch. The central autonomic network: Functional organization, dysfunction, and perspective. Mayo Clinic Proceedings, 68:988–1001, 1993.

[41] J. F. Thayer and R. D. Lane. Claude bernard and the heart–brain connection: Further elaboration of a model of neurovisceral integration. Neuroscience and Biobehavioral Reviews, 33:81–88, 2009.

[42] R. Smith, J. F. Thayer, S. S. Khalsa, and R. D. Lane. The hierarchical basis of neurovisceral integration. Neuroscience and Biobehavioral Reviews, 75:274–296, 2017.

[43] W. J. Freeman. Petit mal seizure spikes in olfactory bulb and cortex caused by runaway inhibition after exhaustion of excitation. Brain Research Reviews, 11(3):259–284, 1986.

[44] C. A. Skarda and W. J. Freeman. How brains make chaos in order to make sense of the world. Behavioral and Brain Sciences, 10(2):161–173, 1987.

[45] I. Tsuda. Toward an interpretation of dynamic neural activity in terms of chaotic dynamical systems. Behavioral and Brain Sciences, 24(5):793–810, 2001.

[46] K. A. McKiernan, J. N. Kaufman, J. Kucera-Thompson, and J. R. Binder. A parametric manipulation of factors affecting task-induced deactivation in functional neuroimaging. Journal of Cognitive Neuroscience, 15:394–408, 2003.

[47] H. Koshino, T. Minamoto, K. Yaoi, M. Osaka, and N. Osaka. Coactivation of the default mode network regions and working memory network regions during task preparation. Scientific Reports, 4:5954, 2014.

[48] V. Menon and L. Q. Uddin. Saliency, switching, attention and control: a network model of insula function. Brain structure and function, 214:655–667, 2010.

[49] G. B. Chand, J. Wu, I. Hajjar, and D. Qiu. Interactions of the salience network and its subsystems with the default-mode and the central-executive networks in normal aging and mild cognitive impairment. Brain Connectivity, 7:401–412, 2017.

[50] J. Van Oort, I. Tendolkar, E. Hermans, P. Mulders, C. Beckmann, A. Schene, G. Fernández, and P. Van Eijndhoven. How the brain connects in response to acute stress: A review at the human brain systems level. Neuroscience and Biobehavioral Reviews, 83:281–297, 2017.

[51] S. Vaisvaser, S. Modai, L. Farberov, T. Lin, H. Sharon, A. Gilam, N. Volk, R. Admon, L. Edry, E. Fruchter, I. Wald, Y. Bar-Haim, R. Tarrasch, A. Chen, N. Shomron, and T. Hendler. Neuro-epigenetic indications of acute stress response in humans: The case of microRNA-29c. PLOS ONE, 11(1):e0146236, 2016.

[52] T. Chand, M. Li, H. Jamalabadi, G. Wagner, A. Lord, S. Alizadeh, L. V. Danyeli, L. Herrmann, M. Walter, and Z. D. Sen. Heart rate variability as an index of differential brain dynamics at rest and after acute stress induction. Frontiers in Neuroscience, 14, 2020.

[53] R. Wilson. Sudoku, last updated 2022. https://www.britannica.com/topic/sudoku.

[54] S. M. Pincus. Approximate entropy as a measure of system complexity. Proceedings of the National Academy of Sciences, 88:2297–2301, 1991.

[55] S. M. Pincus, I. M. Gladstone, and R. A. Ehrenkranz. A regularity statistic for medical data analysis. Journal of Clinical Monitoring, 7:335–345, 1991.

[56] T. Higuchi. Approach to an irregular time series on the basis of the fractal theory. Physica D: Nonlinear Phenomena, 31:277–283, 1988.

[57] H. Ahammer. Higuchi dimension of digital images. PLOS ONE, 6(9):e24796, 2011.

[58] A. H. Rosangela, M. P. Carlos, L. C. M. Vanderlei, and M. F. Godoy. Poincaré plot indexes of heart rate variability: Relationships with other nonlinear variables. Autonomic Neuroscience, 177:271–274, 2013.

[59] P. Guzik, J. Piskorski, T. Krauze, R. Schneider, K. H. Wesseling, A. Wykretowicz, and H. Wysocki. Correlations between the poincaré plot and conventional heart rate variability parameters assessed during paced breathing. The Journal of Physiological Sciences, 57:63–71, 2007.

[60] T. Vybiral, R. J. Bryg, M. E. Maddens, and W. E. Boden. Effect of passive tilt on sympathetic and parasympathetic components of heart rate variability in normal subjects. The American Journal of Cardiology, 63:1117–1120, 1989.

[61] L. A. Lipsitz, J. Mietus, G. B. Moody, and A. L. Goldberger. Spectral characteristics of heart rate variability before and during postural tilt. relations to aging and risk of syncope. Circulation, 81:1803–1810, 1990.

[62] M. Osaka, K. Yaoi, T. Minamoto, and N. Osaka. When do negative and positive emotions modulate working memory performance? Scientific Reports, 3:1375, 2013.

[63] R. N. Spreng. The fallacy of a “task-negative” network. Frontiers in Psychology, 3, 2012.

List of author's papers related to this thesis

1. Tomoyuki Mao, Hidetoshi Okutomi, and Ken Umeno, Investigation of the difference between chaos degree and Lyapunov exponent for asymmetric tent maps, *JSIAM Letters*, **11**(2019), 61–64. (DOI: 10.14495/jsiaml.11.61)

2. 真尾 朋行, 奥富 秀俊, 梅野 健, カオス尺度とリアプノフ指数の差の解釈に基づく修正カオス尺度の提案, 日本応用数理学会論文誌, **29**(2019), 383–394. (DOI: 10.11540/jsiamt.29.4_383)

3. Tomoyuki Mao, Hidetoshi Okutomi, and Ken Umeno, Analysis of the limit values of chaos degree for infinite number of partitions in asymmetric tent maps, *JSIAM Letters* (Conditional accepted on 2022/11/24)

4. Tomoyuki Mao, Hidetoshi Okutomi, and Ken Umeno, Chaotic fluctuations in heart rate variability associated with interaction of large-scale brain networks: experiments and hypotheses, PREPRINT (Version 1) available at Research Square, November 2022. (DOI: 10.21203/rs.3.rs-2190064/v1)

- Chapter 2 is based on papers 1 and 3.
- Chapter 3 is based on paper 2.
- Chapter 4 and Chapter 5 are based on paper 4.

List of Figures

List of Tables